Neurogenesis changes β-catenin shipping address from adherens junctions to nucleus to booster axonal growth

Antonio Herrera[1,*], Anghara Menendez[1], Andrea Ochoa[1], Lídia Bardia[2], Julien Colombelli[2] and Sebastian Pons[1,‡]

[1]Instituto de Biología Molecular de Barcelona (CSIC), Parc Científic de Barcelona, Baldiri Reixac 10-12, Barcelona 08028, Spain.
[2]Institute for Research in Biomedicine (IRB Barcelona), the Barcelona Institute of Science and Technology (BIST), Baldiri Reixac 10, Barcelona 08028, Spain

[*]Present address: Laboratory of Neurodevelopmental Systems Biology, Brain Mind Institute, School of Life Sciences, École Polytechnique Fédérale de Lausanne (EPFL), 1015 Lausanne, Switzerland
[‡]Correspondence author: Sebastian Pons, Instituto de Biología Molecular de Barcelona, (CSIC), Parc Científic de Barcelona, Baldiri Reixac 10-12, Barcelona 08028, Spain. spfbmc@ibmb.csic.es

Abstract

Here we show that in the developing spinal cord (SC), after the early Wnt-mediated Tcf-transcription activation that confers dorsal identity to neural stem cells (NSCs), neurogenesis readdressed β-catenin from the adherens junctions (AJs) to the nucleus to stimulate Tcf-dependent transcription in a Wnt-independent manner. This new β-catenin activity regulates genes implicated in several aspects of contralateral axon growth, including axon guidance and adhesion. Using live imaging of ex-vivo chick neural tube (NT), we show that the nuclear accumulation of β-catenin and the rise of Tcf-dependent transcription both initiate before the dismantling of the AJs, and remain during the axon elongation process. Notably, we demonstrate β-catenin activity in post-mitotic cells depends on *TCF7L2* and is central for spinal commissural axon growth. Together, our results reveal a Wnt independent Tcf/β-catenin regulation of genes that control the growth and guidance of commissural axons in chick SC.

Introduction

During spinal cord (SC) development, canonical Wnt signaling has an essential role in dorso-ventral patterning and proliferation of neural stem cells (NSCs) (Muroyama et al., 2002; Alvarez-Medina et al., 2008; Andrews et al., 2019). Roof plate secreted Wnts binds to receptor Frizzled and co-receptor LRP-5/6 at the membrane of NSCs to release β-catenin from Axin/GSK-3β/APC destruction complex and be translocated into the nucleus. Once in the nucleus, β-catenin forms complexes with Tcf/Lef transcription factors, which bind directly to genomic Tcf/Lef response elements to induce the expression of their target genes (Clevers, 2006; Nusse and Clevers, 2017). However, β-catenin also plays an important role in apical-basal cell polarity of NSCs by contributing to the maturation of N-cadherin and consequently to the establishment of apical adherens junctions (AJs) (Baum and Georgiou, 2011; Herrera et al., 2021). Regionalization of the neural tube (NT) begins early in neurodevelopment, while NSCs proliferate symmetrically in a self-expanding mode. Later on, and in association with the onset of neurogenesis, NSCs change their mode of division to generate the first committed neurons (Gotz and Huttner, 2005; Saade et al., 2013). After neurogenic divisions, post-mitotic NSCs diminish N-cadherin expression and increase *TUBB3* expression before detaching from the proliferative ventricle in a process known as apical abscission (Rousso et al., 2012; Das and Storey, 2014; Sagner et al., 2018). During the first wave of neurogenesis, 11 different populations of spinal neurons are generated: 6 dorsal interneuron populations (dI1-dI6), 3 ventral interneuron populations (V0-V3), and a large number of motor neurons (MNs) (Helms and Johnson, 2003; Lai et al., 2016). The interneuron populations can reach ipsilateral or contralateral targets, these last neurons are known as commissural neurons. Their axons grow towards the floor plate (FP), cross the ventral midline (commissure), and turn following the FP. Then, a large part of them deviates to follow the ventral or lateral funiculi (VF/LF) until reaching their targets (Kadison and Kaprielian, 2004; Chédotal, 2019). Axon guidance signals, including Netrin/DCC, Slit/ROBO, Sonic hedgehog/BOC, EphrinB3/EPHA4, and Wnts/Fzd3, work together to promote the growing and guiding of commissural axons. Floor-plate (FP) Shh and Netrin-1 guide commissural axons to cross the midline by binding to BOC and DCC on pre-crossing commissural axons (Fazeli et al., 1997; da Silva et al., 2018). After crossing the midline, FP-secreted Slit proteins repel commissural growth cones by activating ROBO1 and ROBO2 receptors, preventing them from re-entering the midline (Long et al., 2004; Reeber et al., 2008; Jaworski et

al., 2010). Various Wnt proteins induce the anterior turning and growth of post-crossing commissural axons through Fzd3 receptor (Lyuksyutova et al., 2003; Onishi and Zou, 2017). This is part of the planar cell polarity (PCP) signaling, a pathway that is independent of β-catenin/Tcf/Lef proteins. In addition, guidance pathways coordinate with adhesion molecules such as N-cadherin and integrins to promote directional remodeling of the actin cytoskeleton during axonal growth and pathfinding (Rhee et al., 2002; Myers and Gomez, 2011).

Here we combine the expression of Cre recombinase under the control of a 229 bp proximal element of the *TUBB3* gene promoter region with multiple LoxP vectors to dissect post-mitotic from proliferative β-catenin/Tcf/Lef mediated transcription. We demonstrate that after the initial activation of Tcf-dependent transcription by Wnt proteins that confer dorsal identity to NSCs of chick SC, Tcf-dependent transcription is activated again by a Wnt-independent mechanism in differentiating SC commissural neurons. This second transcription activation controls the expression of genes involved in axon guidance and adhesion required for contralateral axon growth. We used live imaging of ex vivo chick NT to show that β-catenin accumulates in the nucleus just before the dismantling of the AJs that precedes the apical abscission. Nuclear β-catenin then activates Tcf/Lef dependent transcription that remains high during axon elongation. Besides, we show that the downregulation of *TCF7L2* prevents post-mitotic Tcf transcription and severely impairs spinal commissural axon growth. Together, our results reveal a Wnt-independent Tcf/β-catenin regulation of genes that control the growth and guidance of commissural axons in the chick SC.

Results

Tcf/Lef dependent transcription is activated during commissural differentiation in the chick SC.

In ovo electroporation of chick NTs permits genetic manipulations that can be followed during neural development. Now, we have used the thoracic chick SC to study the hitherto unknown Tcf/Lef-dependent transcription activation that occurs coincident with the initiation of neural differentiation. Using a construct expressing membrane GFP (mGFP) under the Top promoter, containing 5 copies of a Tcf/Lef response element (WRE) and a tyrosine kinase (TK) minimal promoter, we electroporated the NTs of E3 (three days post-conception) chick embryos and followed them for 24, 48 or 72 h.

Notably, we observed that in E4 chick SCs, in addition to the dorsal group of NSCs conforming to the Wnt response domain, Tcf/Lef mediated transcription was also active (Top[+]) in dorsal cells with neuronal morphology. Besides, as neurogenesis extended to more ventral regions in E5 and E6, the presence of Top^{+} cells with signs of neural differentiation also extended ventrally (Fig 1A, B). Interestingly, many of these Top^{+} neurons extended axons to the contralateral side through the commissure. During their differentiation, neurons migrate laterally to form the mantle zone (MZ) basal to the ventricular zone (VZ, Fig 1C). Interestingly, we observed that the percentage of Top^{+} cells remained constant from E4 to E6. Moreover, no differences were observed between the VZ and the MZ, suggesting that Tcf/Lef mediated transcription remained active throughout the neural differentiation process (Fig 1D). The dorsal Wnt response domain is already significantly reduced at E5 (Agalliu et al., 2009) (Fig S1A). However, to ensure that the observed Tcf/Lef activity in neurons was not inherited from Wnt-responsive NSCs, we used a Top vector that drives the expression of a GFP containing a PEST sequence at its C-terminus, which reduced its half-life from 20 hours to 2 hours (Li et al., 1998; He et al., 2019). Again, we observed Tcf/Lef activity in ventricular progenitor cells and differentiated neurons (Fig S1B). Neurogenin-1 (Ngn1) is a pro-neural gene that induces premature neuronal differentiation and commissural dI2 subtype specification in SC (Gowan et al., 2001; Alaynick et al., 2011; Le Dreau et al., 2018). We observed that transfection of Ngn1 for 24 h in E2 chick NTs increased the percentage of Top^{+} cells in a cell-autonomous manner (Fig 1E, F). Moreover, transfection of either Ngn1 or p27[Kip1], a cell cycle repressor that induces premature neural differentiation, significantly increased the activity of Top-FLASH, a Tcf/Lef luciferase-reporter. (Fig 1G). Henceforth, the upregulation of Tcf/Lef-dependent transcription observed during neural differentiation will be referred to as "differentiation-associated Tcf/Lef transcription" (DATT). Using an enhancer element from the *TUBB3* gene promoter (Tubb3_enh) (Bergsland et al., 2011), we generated Cre-Lox-based vectors to study and manipulate DATT without altering the pathway in NSCs. In addition, we created two groups of vectors where the transcription of mGFP, driven either by the CAG promoter (b-actin promoter with the CMV[E1A] enhancer) or the Top promoter, was blocked by a floxed poly-adenylating sequence (pA, Fig 1H). The vectors showed good expression and low leakage. (Fig S1C). Co-transfection of Tubb3:Cre with CAG:LoxP·mGFP (Tubb3::CAG:mGFP) showed all the differentiating neurons among the transfected cells (transfection was monitored with H2B·RFP),

whereas co-transfection of Tubb3:Cre with Top:LoxP·mGFP (Tubb3::Top:mGFP) revealed only the Top$^+$ differentiating neurons (Fig 1I and Fig S1D). In E5 chick SCs, the MZ can be further divided into two areas containing the interneurons (IN) and the motoneurons (MC), respectively (Fig 1J). We used anti-Robo3, which labels commissural axons from the cell body to commissure (Fig 1I), to delimitate the IN, the MC, the VZ, and the 3 main axonal tracts containing commissural interneuron projections: the commissure, the contralateral ventral funiculus (VF) and contralateral lateral funiculus (LF; Fig 1J) (Wu et al., 2019). In E5 chick SCs that had been transfected for 24 h, the percentage of Top$^+$ among post-mitotic cells was significantly higher in the VZ and the IN than in the MC (15.7 +/- 3.2% in VZ, 21.77 +/- 5.82 in IN and 3.45 +/- 0.89% in MC; Fig 1I, K). In addition, the VZ/MZ GFP-ratio was significantly higher in Tubb3::Top:mGFP than in Tubb3::CAG:mGFP embryos, indicating that while the CAG activity remained constant during differentiation, the Top activity was higher while the future neurons were still in the VZ (Fig 1I, L). Besides, compared to total transfected neurons (Tubb3::CAG:mGFP), Top$^+$ neurons (Tubb3::Top:mGFP) were more abundant in the dorsal region than in the medial and ventral regions of the VZ (Fig 1M). This result demonstrated that DATT was more abundant in the dorsal SC, but present at other dorso-ventral levels, suggesting that DATT was mostly present in commissural neurons. To test that, we compared GFP fluorescence intensity (FI) in the different axonal tracks of Tubb3::CAG:mGFP and Tubb3::Top:mGFP embryos. Notably, almost 100% of transfected axons were Top$^+$ in the commissure, whereas this percentage was very low in the other tracts except for the ventral contralateral track, where it was moderate (Fig 1N). These results confirmed that the observed Top$^+$ neurons were mostly commissural neurons in which Tcf/Lef-dependent transcription was activated during differentiation.

DATT is required for commissural outgrowth and pathfinding in developing SC.
In the absence of nuclear β-catenin, Tcf/Lefs act as transcriptional repressors by binding to Groucho/TLE proteins (Daniels and Weis, 2005). Expression of β-catenin ^{S33Y}, a stable form of β-catenin (sβ-Cat), induces a potent activation of Tcf-dependent transcription in chick NT, whereas TcfEnR, a fusion of Tcf3 HMG-box (Tcf3 DNA-binding-domain) with the transcriptional repressor engrailed (Eng), drastically reduces it (Herrera et al., 2014). We used the bicistronic CAG:LoxP·mGFP vector to expresses either TcfEnR or sβ-Cat, which combined with Tubb3:Cre produced

Tubb3::CAG:TcfEnR and Tubb3::CAG:sβ-Cat, respectively (Fig S2A). We electroporated E3 chick NTs for 24 h with Tubb3::CAG:TcfEnR or Tubb3::CAG:sβ-Cat. mGFP showed the cell body and projections of transfected cells, whereas anti-Robo3 stained commissural axons. Either suppression or sustained activation of Tcf/Lef dependent transcription reduced commissural axons. However, the effect of sβ-Cat was very moderate compared to the severe reduction caused by TcfEnR (Fig 2A, B). Besides, TcfEnR expression caused ectopic exit of commissural axons through the dorsal root (Fig 2A'). These effects may be cell-autonomous, as total ROBO3 expression was unaffected in the descending commissural tracts (Fig 2C). To evaluate whether Tcf-dependent transcription was required for axon outgrowth, we transfected E3 chick embryos with TcfEnR (Tubb3::CAG:TcfEnR) or control (Tubb3::CAG:mGFP) and 12 h later dissected the dorsal NTs to prepare interneuron cultures (Langlois et al., 2010) (Fig 2D). Notably, we observed that suppression of Tcf/Lef transcription significantly reduced the length of axons after two days in culture (Fig 2E, F).

DATT promotes commissural axon elongation and pathfinding through adhesion and axon guidance pathways.

To study the Tcf-dependent genes that were active during commissural neuron differentiation, we transfected E3 chick embryos for 24 h to produce either Tubb3::CAG:TcfEnR (suppression of Tcf-dependent transcription in neurons) or Tubb3::CAG:control (controls) and cell-sorted the GFP$^+$cells. Then we used Affymetrix GeneChip arrays to study the transcriptomes (Fig 3A). Comparing Tubb3::CAG:TcfEnR transfected embryos with controls, 302 genes were upregulated, and 567 were downregulated (Table 1). The Affymettrix data are in GEO, accession number GSE234518 (see Table 2 for metadata). We were mostly interested in the group of down-regulated genes, assuming that these genes were the ones that, either directly or indirectly, were activated by DATT (Fig 3B). To validate the rationale of this approach, we manually selected a group of genes involved in different aspects of axon outgrowth and guidance (Fig 3B'), and studied their expression by RT q-PCR comparing Tubb3::CAG:TcfEnR to Tubb3::CAG:sβ-Cat, where the pathway was activated by sβ-Catenin. Consistently, the group of genes that were downregulated in Tubb3::CAG:TcfEnR embryos were enhanced by sβ-Catenin, confirming that all the genes in this group were β-Catenin/Tcf-dependent targets (Fig 3C). We further

computationally analyzed the group of downregulated genes (log2 fold change ≤ 2 with adjusted p value ≤0.05) by GO enrichment analysis plus PANTHER classification system to find the pathways affected (Fig 3D) (Ashburner et al., 2000; Mi et al., 2019; Gene-Ontology-Consortium, 2021). Additionally, we used Enrichr (Chen et al., 2013; Kuleshov et al., 2016; Xie et al., 2021) to determine the transcription factors intervening (ENCODE TF; Fig 3E) and the proteins associated with those transcription factors (Transcription Factor PPIs; Fig 3F). PANTHER predicted the signaling pathways of cadherins, integrins, and Wnt proteins to be regulated by DATT with high scores; however, the Slit/Robo axon guidance pathway received the highest score. Although receiving lower scores, the expression of other genes involved in the axon guidance pathways mediated by netrin and semaphorins were also significantly downregulated in Tubb3::CAG:TcfEnR neurons. On the other hand, ENCODE TF database predicted that TCF7L2 (Tcf4) was one of the main transcription factors mediating Tcf-dependent transcription in this process. So, we used pSHIN, a GFP expressing vector, to clone short hairpin inhibitory RNAs (shRNAs) against the different Tcf/Lef transcription factors expressed in E4 chick NTs: LEF1, TCF7, TCF7L1, and TCF7L2 (Fig S2B, C), transfected them in E3 chick NTs for 48 h and stained sections with Tuj1(Fig 4A) or anti-Robo3 (Fig S2D) to study the presence of GFP$^+$ axons in contralateral axonal tracks. Notably, the presence of GFP$^+$ fibers in the commissure and the contralateral VF was significantly reduced after *TCF7L2* suppression compared to the controls or the other knockdowns. (Fig 4B). This effect was not due to the suppression of dorsal patterning previously reported by Wnt/β-catenin pathway inhibition (Fig S2E). Besides, we transfected E3 embryos with the mentioned shRNAs, plus Top Flash reporter and Ngn1 or control vector. As expected, expression of Ngn1 increased Tcf-dependent transcription; however, this increase disappeared with *TCF7L2* suppression (Fig 4C). Among Tcf/Lef transcription factors, TCF7L2 received the highest score by ENCODE TF database in mediating DATT; however, the absolute highest score was given to FOXM1, a transcription factor reported to be required for the neuronal differentiation (Ueno et al., 2008). Nevertheless, suppression of *FOXM1* did not impede the effect of Ngn1 on Tcf-dependent transcription (Fig 4C). Altogether, these results confirmed that DATT regulates the transcription of a set of genes involved in commissural axon elongation and guidance specifically through the TCF7L2 transcription factor. To further assess the effect of *TCF7L2* suppression, we transfected E3 chick embryos for 24 h (E3 + 24 hpe) with pCS2-mRFP plus pSHIN-ShTCF7L2 or pSHIN-ShControl,

whole-mount immuno-labeled them with anti-RFP and anti-Robo3 antibodies, cleared them optically and performed volume imaging through light sheet fluorescence microscopy. Bearing in mind that we only electroporate one side of the neural tube, which we consider to be ipsilateral (Fig 4D), this technique is suitable to reveal perturbations in the ratio of axons occupying ipsilateral versus contralateral axonal tracts. In accordance with the 2D images shown in Fig 4A, the 3D images generated from light-sheet microscopy confirmed that *TCF7L2* knockdown significantly decreased the ratio of axons that crossed and followed the contralateral tract respect to the ones that followed the ipsilateral tract (7.75 +/- 0.35in control versus 0.79 +/- 0.02 in TCF7L2 knock down; Fig 4E, F and movies 5 and 6). Concomitant with the decrease in contralateral axons, an important accumulation of GFP was observed in the somas of pSHIN-ShTCF7L2 transfected cells, but not in the ipsilateral tracts, indicating a defect in the growth of commissural axons rather than a redirecting towards the ipsilateral tracks.

DATT is Frizzled independent and begins before apical abscission.

The canonical Wnt pathway is mediated by its membrane receptor Frizzled, a co-receptor called LRP-5/6 and β-catenin, among others (Fig 5A). We used the Tubb3:Cre system with a dominant negative form of LRP-5/6 (LRPdn; Fig 5B) and a mutant β-catenin with diminished transcriptional activity (sβCatΔC; Fig 5C) to study the implication of Wnt proteins and β-catenin on commissural neuron differentiation. Notably, we observed that cells expressing LRPdn extended axons normally, in spite that the expression of this construct in E2 chick neural tubes clearly inhibited the expression of Top:H2B·RFP in both the dorsal Wnt response domain and the dorsal root ganglia (Fig 5D and S3); in contrast, the number of axons from cells expressing sβCatΔC was significantly reduced in the commissure and the contralateral VF (Fig 5E and S4A). These results indicated that DATT was mediated by β-catenin but not by Wnt proteins. To study the chronology of DATT, we transfected E2 chick embryos for 24 h with Ngn1 to induce differentiation, mGFP to show the cell contour, and Top:H2B·RFP, to monitor Tcf activity. Slices were then stained with anti-β-catenin and DAPI (Fig 5F). We observed transfected dorsal cells at different stages of delamination; cells close to the apical border with NSC morphology (green arrows), cells at basal positions but still attached to the apical border (purple arrows and stars), and cells already delaminated (blue arrows and stars). Top activity (nuclear accumulation of RFP) was higher in delaminated neurons; however, it was already elevated in basal pre-

delaminated cells. Moreover, nuclear accumulation of endogenous β-catenin was evident in these two groups of cells. To better define the time sequence of Top activation during neural differentiation, we transfected E3 embryos for 12 h with Tubb3::Top:mGFP plus H2B·RFP and prepared ex vivo cultures from which we took time-lapse confocal images for a period of 950 min (Fig 5G and movie 1). We calculated the integrated GFP fluorescence density (IFD), which is shown as a percentage of the maximum (Fig 5H). As suggested by fixed tissue experiments, the time-lapse experiments showed that Tcf-dependent transcription raised before apical abscission, then decreased at the beginning of apical foot retraction, and subsequently increased again during neurite formation. In addition, we tracked cells that had already initiated the apical abscission at the beginning of the time-lapse acquisition to study Tcf transcription for as long as possible during axon growth (Fig 5I and movie 2). In this case, we observed the rise in Top activity during neurite formation is also maintained during axon outgrowth and elongation. (Fig 5J). In Fig 5K we summarized in a schematic drawing the observed variation of Tcf-dependent transcription during neural delamination and axon elongation.

β-catenin is readdressed to the nucleus before apical foot abscission during dorsal neural differentiation.

Wnt canonical pathway had been shown to collaborate in the early establishment of dorsal identities during NT development. However, here we have demonstrated that Tcf-dependent transcription is both activated and required during commissural neurogenesis in a process that requires β-catenin but not Wnt proteins. Therefore, we used E5 sections (Fig 6A) to study the distribution of β-catenin mRNA (Fig 6B) and β-catenin protein (Fig 6C). Interestingly, β-catenin mRNA was very abundant at the boundaries between the VZ and the MZ in the dorsal SC, where different populations of interneurons are differentiating at this stage (Fig 6B'). On the other hand, although β-catenin protein was mostly observed with N-cadherin at the AJs of the apical border along the SC, it was also present in most basal locations in the dorsal VZ and the cell bodies of the most dorsal Robo3 expressing neurons (Fig 6C, C'). Besides, β-catenin protein was very abundant in the commissure together with Robo3 (Fig 6C''). In agreement, we observed that in Tubb3::CAG:βCat·FLAG embryos (electroporated at E3 for 24 h), β-catenin·FLAG protein was mainly accumulated in the nucleus and axons of neurons (Fig 6D). During neurogenesis, differentiating neurons detach their apical

process and retract it towards the cell body, leaving a stump where it had been attached (Das and Storey, 2014). Before detachment, N-cadherin levels decrease at the cellular apical pole (Rousso et al., 2012; Das and Storey, 2014). Therefore, we wondered whether DATT was fueled by the β-catenin released during AJs dismantling. We transfected E3 embryos with β-catenin·RFP, mGFP, and Ngn1 for 12h to prepare ex vivo cultures that were followed by confocal time-lapses of the dorsal SC for an additional period of 1050 min (Fig 6E, E', S4B, movies 3 and 4). Initially, β-catenin·RFP was more abundant in the AC than in the nucleus. Later on, it steadily increased in the nucleus without decreasing in the AC, where it remained mostly constant until the apical abscission initiation. Notably, in coincidence with the results of Tcf-dependent transcription shown in Fig 5, nuclear β-catenin·RFP reached its maximum before apical foot abscission, and although it progressively decreased later, it remained substantially elevated during axon outgrowth and elongation (Fig 6F and S4C). In Fig 6G we resume in a schematic drawing the β-catenin·RFP levels observed in the AC and the nucleus before and after apical foot abscission and during axon elongation. The results shown in Figures 5 and 6 demonstrated that both Tcf-dependent transcription and nuclear β-catenin·RFP were raised before the AJs were dismantled. Therefore, we concluded that the rise of nuclear β-catenin, and consequently of Tcf-dependent-transcription, shall depend on a neural-differentiation-prompted mechanism that either readdresses newly produced β-catenin directly to the nucleus or interferes with the destruction complex allowing its nuclear accumulation.

Discussion

β-catenin/Tcf-dependent transcription is reactivated during SC commissural differentiation in a Wnt-independent manner.

Wnt canonical pathway (β-catenin/Tcf dependent) participates in defining dorsal fate and maintains stemness of neural progenitors, whereas its inhibition induces premature cell cycle exit and ventral patterning during the early SC development (Alvarez-Medina et al., 2008; Wang et al., 2011; Herrera et al., 2014). However, we have now demonstrated that later, during the first wave of neurogenesis, β-catenin/Tcf-dependent transcription is reactivated during neuronal differentiation of different subtypes of chick spinal commissural interneurons. Moreover, we have observed that this reactivation is

an absolute requirement for the growth of pre-crossing commissural axons. Similarly, β-catenin/Tcf-dependent transcription is also activated early in the neural precursors of the mouse cortex ventricular zone during radial glial cell expansion, and although it is silenced while these cells exit the ventricular zone and migrate towards the cortical plate, it is later reactivated in a set of young neurons as they mature in the cortical plate (Woodhead et al., 2006). Although the involvement of Wnt proteins in the activation of β-catenin/Tcf-dependent transcription was not studied, the widespread distribution of this set of cortical neurons points against a Wnt factor gradient triggering this activation. In the present study, we demonstrated that, unlike the Tcf repression, the expression of the dominant negative form of the Wnt co-receptor LRP5/6 in Tubb3 expressing cells does not affect the outgrowth and pathfinding of spinal commissural axons. In addition, our experiments in which we overexpress Ngn1 or p27^{Kip1} show that the induction of premature differentiation correlates with an increase in nuclear localization of β-catenin and subsequent β-catenin/Tcf-dependent transcription in differentiating neurons. On the other hand, although Wnt-dependent axon guidance had mainly been attributed to PCP pathway, defects in post-crossing axons have been observed in knock-downs of Lrp5/6 in chick neural tubes, indicating that Wnt canonical pathway may also be participating after midline crossing (Avilés and Stoeckli, 2016). However, the activation of β-catenin/Tcf-dependent transcription in pre-crossing commissural neurons is likely to be an inherent consequence of the differentiation process rather than being influenced by external Wnt proteins.

β-catenin round trip to the nucleus during commissural neuron differentiation.
N-cadherin is responsible for the maintenance of the apical attachment (Wong et al., 2012), and the delamination process is associated with a downregulation of N-cadherin induced by pro-neuronal transcription factors such as neurogenins (Rousso et al., 2012; Das and Storey, 2014). Newly synthesized β-catenin has two possible outputs, it may interact with N-cadherin at the endoplasmic reticulum and travel to the AJs, or be translocated into the nucleus. Downregulation of N-cadherin during neuron delamination could be tipping the scale to the transcriptional output. We have observed that both, nuclear accumulation of β-catenin and DATT, begin without a decrease of β-catenin at the AC. Thus, although the downregulation of N-cadherin could be involved, the AJs do not seem to be the primary source of the β-catenin that accumulates in the nucleus during commissural neuron differentiation. Our data show that DATT is

activated during neuron delamination, continues active in pre-crossing commissural axons, and eventually is turned down in post-crossing commissural axons. Therefore, it is most likely that different concurrent and sequential events may regulate the nuclear accumulation of β-catenin during the process of differentiation. On the one hand, in the mouse cerebral cortex, the expansion of intermediate progenitors (IPs) depends on the interaction of Axin with Gsk3b in the cytoplasm. However, as neural differentiation begins, Axin is phosphorylated by β-catenin-associated Cdk5, causing the nuclear translocation of the Axin/β-catenin complexes and the activation of Tcf-dependent transcription. Interestingly, both nuclear accumulation of Axin/β-catenin and Tcf-dependent transcription are required to promote the differentiation of IPs into neurons (Fang et al., 2013). Therefore, an equivalent mechanism may also be driving β-catenin to the nucleus during commissural neuron delamination. Besides, Slit interacts with Robo to induce the association of Robo/Abl complex with β-catenin/N-cadherin/Cables, causing the phosphorylation of β-catenin at Y489 by Abl that dissociates from N-cadherin and accumulates in the nucleus (Rhee et al., 2007). Thus, the induction of Robo1 and Robo2 expression by DATT may contribute to the maintenance of β-catenin/Tcf-dependent transcription in pre-crossing commissural neurons. On the other hand, a midline crossing mechanism that depends on the accumulation of β-catenin at the axon growth cone has been recently reported during midline crossing at the optic chiasm (Morenilla-Palao et al., 2020). In the suggested model, the differential expression of Wnt receptors would determine the effect of midline-expressed Wnt5a on the decision to cross the midline by commissural axons or be repulsed in the case of ipsilateral axons. While the expression of Fzd1, Fzd8, and Lgr5 induced by Zic2 in ipsilateral neurons avoids the midline crossing by promoting a non-polarized distribution of β-catenin, other Wnt receptors such as Fzd3 have been proposed to respond to Wnt5a and mediate the required accumulation of β-catenin at commissural growth cones during midline crossing. Interestingly, our data have revealed an accumulation of β-catenin in midline Robo3^{+} axons and a positive regulation of Fzd7 and Fzd3 expression by DATT in spinal commissural neurons. The interaction of floor plate Wnt5a with some of these Wnt receptors may promote the accumulation of β-catenin at midline crossing growth cones and, therefore, the shutdown of the transcriptional signal in post-crossing axons. In summary, different mechanisms may operate from the initial steps of neural differentiation to the post-crossing stages in commissural neurons.

The growth of pre-crossing commissural axons depends on genes activated by DATT during SC development.

At the end of the 19th century, Ramón y Cajal proposed that floor plate cells secreted attractants for commissural axons that extend ventrally in the developing SC. To date, three floor-plate-derived chemo attractive factors have been identified, Netrin-1 (Kennedy et al., 1994), Sonic hedgehog (Shh) (Charron et al., 2003), and vascular endothelial growth factor (VEGF) (Ruiz de Almodovar et al., 2011). However, only Netrin-1 promoted the growth of axons and was required for the midline crossing (Moreno-Bravo et al., 2019; Wu et al., 2019). PANTHER pathway analysis informs that DATT positively regulates cell adhesion and axon guidance genes relevant during commissural neuron differentiation. Different receptors interact with Netrin-1, such as DCC, UNC5C, Neo1, and ROBO3 (Chédotal, 2019), and midline crossing by commissural axons is drastically reduced in mutant mice in which Netrin-1, DCC, or Robo3 are deleted (Serafini et al., 1996; Fazeli et al., 1997; Long et al., 2004). Besides, although commissural axon crossing is normal in a severe hypomorphic Neo1mouse model, it potentiates the effects caused by deleting DCC (Xu et al., 2014). The phenotype we observed after the suppression of Tcf-dependent transcription in chick SC is very similar to the one reported for DCC deletion, despite the fact that the DCC gene is lost in birds from the chicken family (Patthey et al., 2017). Interestingly, Neo1 mRNA is expressed in developing chick SC in a pattern resembling mouse DCC rather than Neo1, suggesting that in chicken, the functions of DCC may have been assumed by Neo1 (Phan et al., 2011). Notably, Neo1 was one of the genes whose expression was significantly downregulated after Tcf transcription inhibition. On the other hand, Slit/Robo pathway is required for the correct axon guidance of post-crossing commissural axons through a repulsive mechanism exerted by Slit proteins secreted by the floor plate (Chédotal, 2019). In accordance, midline crossing is perturbed in Slit1, Slit2, and Slit3 triple KO (Long et al., 2004) or Robo1 and Robo2 double KO (Jaworski et al., 2010). Here we have shown that DATT induces the expression of genes classified by PANTHER-pathway into the category called "axon guidance mediated by Slit/Robo". Robo1 and Robo2 are expressed early in pre-crossing commissural axons; however, Robo3 increasingly quenches their presence in the growth cones of these commissural axons as they approach the midline to allow its crossing, being re-established after crossing to avoid the re-entering. Although much attention has been devoted to the repulsion effect that midline-located Slit produces on post-crossing axons

that express Robo1 and Robo2, the lack of motor column avoidance by the descending commissural axons in Slit and Robo KO mice demonstrates a function of Slit/Robo system in pre-crossing axon guidance (Long et al., 2004; Jaworski et al., 2010). Remarkably, in stage HH16-17 chick SC (equivalent to 9.5 in mice), where most interneurons are still initiating the axon extension process, Robo1 and Slit2 mRNAs are abundant in the areas occupied by the cell bodies of dorsal interneurons and the motor neurons, respectively (Mambetisaeva et al., 2005). Besides, in addition to its function in axon guidance, Robo1 has also been demonstrated to control the balance between direct and indirect neurogenesis in the differentiation of the cerebral cortex (Cárdenas et al., 2018). In addition, the PANTHER pathway analysis showed the cadherin signaling pathway as the second pathway with the highest combined score. Interestingly, N-cadherin dysregulation alters commissural projections in the SC; its overexpression seriously affected the navigation of post-crossing commissural axons, and its knockdown significantly reduced the presence of commissural axons (Yang et al., 2016). Our *in silico* analysis predicted *TCF7L2* as one of the main transcription factors regulating the aforementioned PANTHER pathways. Besides, in our study *TCF7L2* knockdown entirely reproduced the phenotype induced by the suppression of TCF-dependent transcription. Similarly, the pathfinding defects of the thalamocortical axons of forebrain-specific *TCF7L2* deficient mice were attributed to the downregulation of cell adhesion and axon guidance genes during the thalamic and habenular neuron differentiation (Lee et al., 2017; Lipiec et al., 2020). In addition, the Neurod6:Ctnnb1[Ex3] mouse, which expressed a stabilized form of β-catenin during the differentiation of cortical excitatory neurons, presented as the main phenotype a lack of the hippocampal commissure (Morgan-Smith et al., 2014). In summary, our data and the abovementioned studies indicate that the genes regulated by β-catenin/TCF7L2 play important roles in axon pathfinding during neuronal differentiation.

Materials and methods

Commercial antibodies and chemicals

The following antibodies and reagents were used in these studies, the concentration indicated is the one used for immunohistochemistry:

Mouse antibodies against β-Catenin (Sigma #C7207; 1:200), Tubulin β-III-Tuj1(Covance # MMS-435P; 1:5000)

Rabbit antibodies against Sox2 (Invitrogen #48-1400; 1:500), RFP (Our lab #Rb2; 1:5000)

Goat antibodies against Robo3 (R&D #AF3076; 1:500)

Chemicals - Rhodamine-Phalloidin (Invitrogen, #R415; 1:250).

DNA constructs

Protein expression:

pCIG (CMV-IE enhancer/b-actin promoter- IRES-nuclear GFP)

pCS2-mRFP (CMV-IE94 promoter membrane RFP)

Tubb3:Cre (TUBB3 enhancer/TK minimal promoter-CRE)

CAG:LoxP·mGFP (b-actin promoter/CMV-IE enhancer-Lox-PolyA-Lox-IRES-mGFP)

Top:LoxP·mGFP (5xWnt response element/TK minimal promoter-Lox-PolyA-Lox-IRES-mGFP)

CAG:LoxP·TcfEnR (Fusion of engrailed repressor to Tcf3 HMG box, cloned in CAG:LoxP·mGFP)

CAG:LoxP·sβCat·mGFP (β-catenin^{S33Y} cloned in CAG:LoxP·mGFP)

CAG:LoxP·LRPdn. (LRP-6 with a C-terminus deletion cloned in CAG:LoxP·mGFP)

CAG:LoxP· sβCatΔC (β-catenin^{S33Y} with a C-terminus deletion cloned in CAG:LoxP·mGFP)

TopFlash (5xWnt response element/TK minimal promoter luciferase)

Top:mGFP (5xWnt response element/TK minimal promoter membrane-GFP)

Top:dGFP (5xWnt response element/TK minimal promoter dGFP)

Top:H2B·RFP (5xWnt response element/TK minimal promoter Histone2b·RFP)

Short Hairpin inhibitory RNAs:

pSHIN (H1 promoter for shRNAs plus SRα promoter for EGFP).

Targeted sequences:

```
shScrambled CCGGTCTCGACGGTCGAGT (Control Sh)
shLEF1      CCCAGAACATCCAACAAGG
shTCF7      CGCGGGACAACTACGGAAA
shTCF7L1    ATGGGCGATGAAGCCAGGA
shTCF7L2    TGAGCACTTCACACCAGGA
```

```
shFOXM1        GCATCAACTCCTACCTTGT
```

Affymetrix GeneChip arrays

Plasmid DNA encoding Tubb3:Cre and either CAG:LoxP·mGFP or
CAG:LoxP·TcfEnR were co-electroporated into E3 chicken embryos for 24 h to
produce either Tubb3::CAG:TcfEnR (suppression of Tcf-dependent transcription in
neurons) or Tubb3::CAG:control (controls).

Then, GFP+ neural tubes were dissected out of the embryos under a fluorescence
dissection stereomicroscope. For each experimental replicate, 20-25 dissected NT of
the same conditions were pooled, and a single-cell suspension was obtained following
10-15 min incubation with trypsin-EDTA (Sigma). GFP fluorescent cells were sorted
using FACS Aria III cell sorter (BD Biosciences). After cell sorting, total RNA was
extracted by RNeasy Micro Kit (Quiagen 74004) according to the manufacturer's
instructions. The quality and quantity of purified RNA were verified by Agilent
Bioanalyzer 2100, and subsequently, the RNA was hybridized and processed in
accordance with the manufacturer's instructions (Affymetrix GeneChip Chicken
Genome Array). The data was processed with the RMA algorithm. The data from three
biological replicates of each experiment were averaged, and differentially expressed
genes were selected. The results were filtered using thresholds of [log2FC]$\geqq$2 (EnR up-
regulated genes) or [log2FC] $\leqq$-2 (EnR down-regulated genes) and q-value (adjusted P
value) $\leqq$0.05. Affymettrix data are in GEO, accession number GSE234518.

Chick embryo *in ovo* electroporation

Eggs from White-Leghorn chickens were incubated at 37.8 °C in an atmosphere of 45%
humidity and the embryos were staged according to Hamburger and Hamilton (HH:
(Hamburger and Hamilton, 1992). Chick embryos were electroporated with column
purified plasmid DNA in H_2O containing Fast Green (0.5 µg/µl). Briefly, plasmid DNA
was injected into the lumen of HH12 (E2) or HH18 (E3) NTs, electrodes were placed on
either side of the NT, and electroporation was carried out by applying five 50 ms square
pulses using an Intracel Dual Pulse (TSS10) electroporator set at 25 V. Transfected
embryos were allowed to develop to the specific stages and then dissected under a
fluorescence dissecting microscope. In our conditions, HH12 embryos electroporated
for 24, 36, and 48 h typically reached stages HH18, HH21, and HH23, respectively;
HH18 embryos electroporated for 24 h and 24 h reached stages HH23 and HH26,

respectively. Embryos that did not develop to the expected stages were discarded. To stage the different embryos we used the staging guide published in: https://embryology.med.unsw.edu.au/embryology/index.php/Hamburger_Hamilton_Stages

Immunostaining and confocal fluorescence microscopy

Embryos were fixed overnight at 4 °C in 4% PFA (4% paraformaldehyde in PBS) and then sectioned at 60μm thickness with a Vibratome (VT1000S, Leica). Immunostaining was performed following standard protocols. The entire procedure was carried out using PBT-BSA (PBS containing 0.1% Triton X-100, 0.1% BSA, and 0.05% sodium azide) using a gently rocking platform. Sections were pre-washed for 30 min at r/t, incubated o/n at 4ºC with primary antibodies, washed three times for 20 min, incubated for 2h at r/t with Alexa or Cyanine conjugated secondary antibodies, washed three times, and mounted with Fluoromount (Sigma-Aldrich). Slices were examined at 18 ºC on a Leica SP5 (20x NA 0.7, 40x NA 1.25) controlled under the Leica LAS software or a Zeiss Lsm 780 (25x NA0.57, 40x NA 1.3, 63x NA0.18) multiphoton microscope controlled under the LSM Software ZEN 2.1. Images were manipulated using Image-J software.

Ex vivo chick NT slice culture and time-lapse imaging

Embryos were electroporated at stage HH18 (E3). After 24 hours of incubation, GFP transfected areas were dissected in ice-cold L15 medium (Sigma L4386) and embedded in 3% low-gelling-temperature agarose dissolved in neurobasal medium (Invitrogen) to be later sectioned at 250 μm thickness with a vibratome (VT1000S, Leica). Next, selected sections were placed on a 35 mm glass-bottom Petri dish (Ibidi) and embedded in 0.5% low-gelling-temperature agarose dissolved in neurobasal medium. Slices were cultured in 2 ml of neurobasal medium supplemented with B-27 (ThermoFisher #17504044) containing 2mM L-glutamine. For time-lapse imaging, images were acquired every 5 min (160 Z planes spaced 0.93 μm, images of 1565x1024 pixels) with a Dragonfly 500 (Oxford Instruments) using a 20X objective (NA 0.75; Fig 5G and movie 1) or every 10 min (20-25 Z planes spaced 1.5 μm, images of 1024x1024 pixels) with a Zeiss LSM780 confocal microscope using a 25X objective (NA 0.80; Fig 5I, Fig 6E, Fig S3B and movies 2,3 and 4) . The culture was maintained at 37.5 ºC in a humid atmosphere (95% air, 5% CO_2). Images were processed with the ImageJ/Fiji software.

Whole-mount immunolabelling and optical clearing

HH18 (E3) chick embryos were electroporated for 24 h (E3 + 24 hpe) with pCS2-mRFP plus pSHIN-ShTCF7L2 or pSHIN-ShControl. Embryos were collected in ice-cold PBS, blood was drained out and extraembryonic membranes removed. Clean embryos were fixed overnight in 4% PFA at 4°C in a rotating wheel and for 1h at room temperature (RT), and finally washed 3 times for 1 h each with PBS. Whole-mount immunolabelling was carried out by a modification of iDISCO protocol (Renier et al., 2014).

Pre-treatment: embryos were then dehydrated through freshly prepared methanol/PBS series (25%, 50%, 75% and finally 100% twice), 1h each at RT. Next, embryos were bleached overnight at 4°C with ice-cold methanol containing 5% H_2O_2 and 20% DMSO. After that, embryos were washed at RT three times in methanol for 1h each, once in methanol containing 20% DMSO for 2h, and rehydrated in freshly prepared methanol/PBS series (75%, 50%, 25% and 0%) 1h each at RT. Finally embryos were washed at RT twice with PBS containing 0.2% TritonX-100 for 1 h each before immunostaining.

Immunostaining: Pre-treated embryos were incubated in PBS containing 0.2% TritonX-100, 20% DMSO and 0.3M glycine overnight at 37°C in a shaker at 80 rpm. Next day, embryos were blocked with PBS containing 0.2% TritonX-100, 10% DMSO and 6% FBS at 37°C in a shaker at 80 rpm for 1 day. Then, embryos were washed twice in PBS containing 0.2% Tween-20 and 10 µg/ml heparin (PTwH) for 1h each. After that embryos were incubated with primary antibodies overnight at 37°and 80 rpm, in PTwH containing 5% DMSO and 3% FBS (goat anti Robo3 at 1:300 and rabbit anti RFP at 1:300). Next day, embryos were washed in PTwH for 10min, 15min, 30min, 1h, 2h and 4h and then incubated with the secondary antibodies in PTwH contain 3% FBS overnight at 37°C and 80 rpm (anti Rabbit Alexa555 and anti Goat Alexa647 at 1:300). Finally embryos were washed in PTwH for 10min, 15min, 30min, 1h, 2h and 4h stored at 4°C in PBS before clearing.

Optical Clearing: After washing with PBS for 30 minutes, chick embryos were embedded into a 0.8% solution of low-melting agarose (A9045, Sigma-Aldrich) diluted in MilliQ water to enable easy mounting of the sample in our custom lightsheet system. We use a 5ml syringe as a mould for that. For refractive index (RI) matching between the sample and the embedding agarose, the blocks containing the tissue were first dehydrated with 3 incubation changes of methanol 100% at 4°C and finally immersed in

a 1:2 mixture of Benzyl Alcohol (2412-1l, Sigma-Aldrich) and Benzyl Benzoate (W213802-1KG-W, Sigma-Aldrich; BABB), at RT for 2-3 days before imaging.

Light sheet fluorescence microscopy.

Once RI was matched, three-dimensional imaging of the entire tissue was carried out using light sheet fluorescence microscopy. For the mesoscopic analysis of the embryos, light sheet fluorescence macroscopy based on a custom instrument (MacroSPIM) was used (Kennel et al., 2018). In brief, the agarose block containing the embryo was placed vertically on an underlying rotation platform inside a 2mm wall quartz cuvette, and immersed in BABB. Imaging was performed horizontally with a AZ100M macroscope lens system (Nikon, Japan) at a magnifications of 9.6x, yielding respective pixel size $XY = 0.677\mu m$, and with Z steps of 2.5µm. The light sheet waist was adjusted to yield around 4.5 to 5 µm of axial resolution. Fluorescence of Alexa555 was excited with a 561 nm DPSS laser, and collected with a "brightline" filter BP609/54, and fluorescence of Alexa647 was induced with a 638 nm solid state laser, collected with a "Edge basic" 635 LP (Semrock filters). Images were generated by a Flash4.0 v2 SCMOS camera (Hamamatsu, Japan). 3D reconstruction images were generated using ImageJ/Fiji software.

Chick embryonic fibroblasts (CEFS) cultures and electroporation.

CEFS were obtained from chick embryos at stage HH30-35 (7-9 days of development). The embryos were mechanically disaggregated with forceps and then treated with trypsin-EDTA for 15 minutes at 37 °C, DNAse I (final concentration 100U/ml) was added to digest the DNA resulting from cell damage, trypsin was inactivated by adding one volume of culture medium with 10% FBS. The cell suspension was centrifuged for 5 minutes at 300 g to eliminate aggregates, and the supernatant was resuspended in Opti-MEM™ (ThermoFisher #31985062) at the desired cell concentration. For electroporation CEFs were resuspended at 15,000,000 cells/ml. Cell cultures were maintained in an atmosphere of 5% CO2 at 37 °C.

Transient transfection of CEFs was carried out with an electroporator (Microporator MP 100, Digital Bio, Seoul, Korea) applying a pulse of 1200-1400V for 20 ms. Transfected cells were seeded according to the experiment to be carried out. For real-time PCR (RT-qPCR) experiments, 1.5-3 million cells per well were seeded in 6-well culture plates and grown for 24 hours.

In situ hybridization

HH18 chick embryos were fixed overnight at 4ºC with 4% PFA. The next day, embryos were dehydrated with increasing concentrations of methanol (25%, 50%, 75%, and 100%) in PBT buffer (PBS containing 0.1% of Tween-20) until the moment of performing the procedure. Whole-mount in situ hybridization was performed following standard procedures. To detect chick CTNNB1 mRNA the following 1046 bp probe was used:

```
   1 CGAGACAGCG GATCTTGGAC TTGACATTGG TGCCCAGGGA GAACCTCTTG GATACCGCCC
  61 AGATGATCCT AGCTACCGTT CTTTCCACTC TGGCGGATAC GGTCAGGATG CCTTGGGTAT
 121 GGACCCTATG ATGGAACATG AAATGGGTGG CCACCACCCT GGTGCTGACT ACCCAGTTGA
 181 TGGTCTGCCA GATCTTGGCC ATGCCCAGGA CCTTATGGAT GGGCTGCCTC CAGGTGACAG
 241 TAATCAGTTG GCCTGGTTCG ATACTGACCT GTAAATCATC CTTTAGCTGT ATCATCTGAA
 301 TGAACTTGCA TTGATTGGCC TGTAGAGTTG CTGAGAGGGC TCGAGGGGTG GGCTAGTATC
 361 TCAGAAAGTG CCTGACACAC TAACCAAGCT GAGTTTCCTA TGGGAACAAT TGAAGTAAAC
 421 TTTTTGTTCT GGTCCTTTTT GGTCGAGGAG TAATAATACA AATGGATTTT GGGAGTGATT
 481 CAAGAAACGA GGAATGCACA AGAATGAATT GCAAGATGGA ATTTATCAAA CCCTAGCCTT
 541 GCTTGTTAAA AATTTATTAT TTTTTTTAAA TCTCTGTAAT GGTACTGACC TTTGCTTGCT
 601 TTGAAAGTAG CCTTTCTTTT CGCAGTAATT GTTGTTAGGT TTTTTTTTTT AAGTCTCTCG
 661 TAGTATTAAG TTATAGTGAA TATGCTACAG CAGTTTCTAA TTTTTAAGGA TTGAGTAAAG
 721 GTGTAGAACA CTAATTCATA ATCGCTCTAA CTGTATTCTG AATAAAGTGT AACATTGTGT
 781 AGCCTTTTTG TATAAAAAAA CTAGACAAAT AGAAATGGTC CAATTAGTTT CCTTTTTAAT
 841 ATGCTTAAAA TAAGCAGGTG GATCTATTTC ATGTTTTTGA TCAAAAACTT TATCTGGGAT
 901 ATGTCTGGGT AGGGGCCAGT AAGAACTGTT TATTTGGAAC CTTGTATTGG ACAGTTTACC
 961 AGTTGCCTTT TATCCCAAAG TTATTGTAGC CTGCTGTGAT ACAGATGCTT CATGAGAAAA
1021 ATGCAGTTAT AAAATGGTTC AAAATT.
```

The probes to detect chick LEF1, TCF7, TCF2L1, and TCF7L2 mRNAs were gently provided by Dr Elisa Marti (Alvarez-Medina et al., 2008). Hybridized embryos were post-fixed in 4% PFA, embedded in 5% agarose - 10% sucrose blocks, and then sectioned with a Vibratome (VT1000S, Leica) at 60μm thickness. Sections were photographed with Olympus DP72 digital color camera attached to a Nikon E600 microscope. The data show a representative image obtained from three embryos.

In vivo luciferase-reporter assay

Embryos were electroporated with the DNAs indicated together with a 5xTcf-BS luciferase reporter construct containing synthetic TCF binding sites (TopFlash), as well as with a renilla-construct (Promega) for normalization. GFP-positive NTs were dissected out at 48 hpe and homogenized in Passive Lysis Buffer. Firefly- and renilla-luciferase activity was measured by the Dual Luciferase Reporter Assay System (Promega).

Immunofluorescence intensity quantification in fixed tissue slices.

Five or six successfully transfected embryos were always used to generate the slices used for quantification. To avoid bias during image acquisition for parameter quantification, we implemented a coding system that concealed the true identity of each image until after analysis. The images were acquired using the same gain and laser parameters. In order to compare the fluorescence intensity in the axons of different compartments, specifically funiculi and commissure, across different treatments, and to make it independent of the transfection level, it was crucial to reference it to the fluorescence measured in the somas of the neurons that emitted the axons. To define the soma regions, both Robo3 and Tuj1 staining were utilized. For each area of interest, the area, integrated density, and mean grey value were measured. Three neighboring selections with no fluorescence were also measured for background readings. The areas of interest were delineated using the freehand line tool in ImageJ/Fiji, with ROBO3 or Tuj1 staining as references. To normalize the intensity of GFP fluorescence in the axons, the following formula was used:

Normalized GFP intensity in axons = (GFP intensity in axons within the region of interest - Mean fluorescence of background readings) / (GFP intensity in somas within ROBO3+ or Tuj1 region - Mean fluorescence of background readings).

First, the mean GFP intensity in the axons within the region of interest was measured, with the average background fluorescence subtracted. Then, the mean GFP intensity in the soma of commissural cells (within the ROBO3+ or Tuj1 region) was calculated, also with the average background fluorescence subtracted. Finally, the first value was divided by the second value to obtain the normalized GFP intensity in the axons.

Fluorescence intensity quantification in ex vivo time-lapse.

For Top-GFP fluorescence quantification (Fig 5H and J), the Z-planes containing the entire studied cell were manually selected and flattened into a single 2D image per each time point. A region of interest (ROI) was defined manually for the entire time sequence and the background was subtracted with ImageJ built-in rolling ball algorithm using a rolling ball radius of 25 pixels (0.34 um/pixel). The integrated fluorescence density (IFD) of the ROI was measured with ImageJ and represented as the percentage of the maximum. For β-catenin·RFP fluorescence quantification (Fig 6F and S4C), ROIs containing the apical pole and the nucleus were manually defined for each time point. The mean fluorescence intensity of the mentioned ROIs and three neighboring

selections with no fluorescence (background measurements) were calculated with ImageJ for the β-catenin·RFP channel at each time point. β-catenin·RFP IF was generated by calculating the mean β-catenin·RFP intensity within the region of interest after subtracting the background.

Statistical Analyses

GraphPad Prism 6 software was used for statistical analysis. A normality study of the data was carried out in all experiments through the D'agostino & Pearson test. For statistical analysis, different statistical tests were used depending on the nature of the data to be compared as suggested by GraphPad Prism build in assistance:

Unpaired t-test was used in Fig 1F, 1L, 2F, 4F and S2C.

Multiple t-tests in Fig 3C.

One-way ANOVA plus Dunn´s multi-comparisons test was used in Fig 1G.

One-way ANOVA plus Tukey´s multi-comparisons test was used in Fig 1K.

One-way ANOVA plus Dunnett´s multiple comparisons test was used in Fig 2C and 4C.

Two-way ANOVA plus Sidak´s multi-comparisons test was used in Fig 1D and 1M.

Two-way ANOVA plus Tukey's multi-comparisons test was used in Fig 1N.

Two-way ANOVA plus Dunnett´s multiple comparisons test was used in Fig 2B, 3C, 4B, and 5E.

Quantitative data with normal distribution are expressed as the mean $\pm$ standard error of the mean (SEM). In all cases a degree of significance was established p-value <0.05: (*), p-value <0.01 (**), p-value <0.001 (***), $p <0.0001$ (****). A confidence limit greater than 95% was established.

Acknowledgments

Author Contributions

A.H. conceived and performed most experiments, analysed the data, discussed the results, and wrote the manuscript. A.O performed experiments and discussed the results. A.M. performed experiments and provided technical support for all the experiments. S.P. conceived experiments, discussed the results, and wrote the manuscript. L.B. performed sample preparation, J.C. performed light sheet imaging.

Declaration of Interests

The authors have no competing financial interests to declare.

Bibliography

Agalliu, D., Takada, S., Agalliu, I., McMahon, A. P. and Jessell, T. M. (2009) 'Motor neurons with axial muscle projections specified by Wnt4/5 signaling', *Neuron* 61(5): 708-20.

Alaynick, W. A., Jessell, T. M. and Pfaff, S. L. (2011) 'SnapShot: spinal cord development', *Cell* 146(1): 178-178 e1.

Alvarez-Medina, R., Cayuso, J., Okubo, T., Takada, S. and Marti, E. (2008) 'Wnt canonical pathway restricts graded Shh/Gli patterning activity through the regulation of Gli3 expression', *Development* 135(2): 237-47.

Andrews, M. G., Kong, J., Novitch, B. G. and Butler, S. J. (2019) 'New perspectives on the mechanisms establishing the dorsal-ventral axis of the spinal cord', *Curr Top Dev Biol* 132: 417-450.

Ashburner, M., Ball, C. A., Blake, J. A., Botstein, D., Butler, H., Cherry, J. M., Davis, A. P., Dolinski, K., Dwight, S. S., Eppig, J. T. et al. (2000) 'Gene ontology: tool for the unification of biology. The Gene Ontology Consortium', *Nat Genet* 25(1): 25-9.

Avilés, E. C. and Stoeckli, E. T. (2016) 'Canonical wnt signaling is required for commissural axon guidance', *Dev Neurobiol* 76(2): 190-208.

Baum, B. and Georgiou, M. (2011) 'Dynamics of adherens junctions in epithelial establishment, maintenance, and remodeling', *J Cell Biol* 192(6): 907-17.

Bergsland, M., Ramsköld, D., Zaouter, C., Klum, S., Sandberg, R. and Muhr, J. (2011) 'Sequentially acting Sox transcription factors in neural lineage development', *Genes Dev* 25(23): 2453-64.

Cárdenas, A., Villalba, A., de Juan Romero, C., Picó, E., Kyrousi, C., Tzika, A. C., Tessier-Lavigne, M., Ma, L., Drukker, M., Cappello, S. et al. (2018) 'Evolution of Cortical Neurogenesis in Amniotes Controlled by Robo Signaling Levels', *Cell* 174(3): 590-606 e21.

Clevers, H. (2006) 'Wnt/beta-catenin signaling in development and disease', *Cell* 127(3): 469-80.

Charron, F., Stein, E., Jeong, J., McMahon, A. P. and Tessier-Lavigne, M. (2003) 'The morphogen sonic hedgehog is an axonal chemoattractant that collaborates with netrin-1 in midline axon guidance', *Cell* 113(1): 11-23.

Chédotal, A. (2019) 'Roles of axon guidance molecules in neuronal wiring in the developing spinal cord', *Nat Rev Neurosci* 20(7): 380-396.

Chen, E. Y., Tan, C. M., Kou, Y., Duan, Q., Wang, Z., Meirelles, G. V., Clark, N. R. and Ma'ayan, A. (2013) 'Enrichr: interactive and collaborative HTML5 gene list enrichment analysis tool', *BMC Bioinformatics* 14: 128.

da Silva, R. V., Johannssen, H. C., Wyss, M. T., Roome, R. B., Bourojeni, F. B., Stifani, N., Marsh, A. P. L., Ryan, M. M., Lockhart, P. J., Leventer, R. J. et al. (2018) 'DCC Is Required for the Development of Nociceptive Topognosis in Mice and Humans', *Cell Rep* 22(5): 1105-1114.

Daniels, D. L. and Weis, W. I. (2005) 'Beta-catenin directly displaces Groucho/TLE repressors from Tcf/Lef in Wnt-mediated transcription activation', *Nat Struct Mol Biol* 12(4): 364-71.

Das, R. M. and Storey, K. G. (2014) 'Apical abscission alters cell polarity and dismantles the primary cilium during neurogenesis', *Science* 343(6167): 200-4.

Fang, W. Q., Chen, W. W., Fu, A. K. and Ip, N. Y. (2013) 'Axin directs the amplification and differentiation of intermediate progenitors in the developing cerebral cortex', *Neuron* 79(4): 665-79.

Fazeli, A., Dickinson, S. L., Hermiston, M. L., Tighe, R. V., Steen, R. G., Small, C. G., Stoeckli, E. T., Keino-Masu, K., Masu, M., Rayburn, H. et al. (1997) 'Phenotype of mice lacking functional Deleted in colorectal cancer (Dcc) gene', *Nature* 386(6627): 796-804.

Gene-Ontology-Consortium (2021) 'The Gene Ontology resource: enriching a GOld mine', *Nucleic Acids Res* 49(D1): D325-D334.

Gotz, M. and Huttner, W. B. (2005) 'The cell biology of neurogenesis', *Nat Rev Mol Cell Biol* 6(10): 777-88.

Gowan, K., Helms, A. W., Hunsaker, T. L., Collisson, T., Ebert, P. J., Odom, R. and Johnson, J. E. (2001) 'Crossinhibitory activities of Ngn1 and Math1 allow specification of distinct dorsal interneurons', *Neuron* 31(2): 219-32.

He, L., Binari, R., Huang, J., Falo-Sanjuan, J. and Perrimon, N. (2019) 'In vivo study of gene expression with an enhanced dual-color fluorescent transcriptional timer', *Elife* 8.

Helms, A. W. and Johnson, J. E. (2003) 'Specification of dorsal spinal cord interneurons', *Curr Opin Neurobiol* 13(1): 42-9.

Herrera, A., Menendez, A., Torroba, B., Ochoa, A. and Pons, S. (2021) 'Dbnl and β-catenin promote pro-N-cadherin processing to maintain apico-basal polarity', *J Cell Biol* 220(6).

Herrera, A., Saade, M., Menendez, A., Marti, E. and Pons, S. (2014) 'Sustained Wnt/beta-catenin signalling causes neuroepithelial aberrations through the accumulation of aPKC at the apical pole', *Nat Commun* 5: 4168.

Jaworski, A., Long, H. and Tessier-Lavigne, M. (2010) 'Collaborative and specialized functions of Robo1 and Robo2 in spinal commissural axon guidance', *J Neurosci* 30(28): 9445-53.

Kadison, S. R. and Kaprielian, Z. (2004) 'Diversity of contralateral commissural projections in the embryonic rodent spinal cord', *J Comp Neurol* 472(4): 411-22.

Kennedy, T. E., Serafini, T., de la Torre, J. R. and Tessier-Lavigne, M. (1994) 'Netrins are diffusible chemotropic factors for commissural axons in the embryonic spinal cord', *Cell* 78(3): 425-35.

Kennel, P., Teyssedre, L., Colombelli, J. and Plouraboué, F. (2018) 'Toward quantitative three-dimensional microvascular networks segmentation with multiview light-sheet fluorescence microscopy', *J Biomed Opt* 23(8): 1-14.

Kuleshov, M. V., Jones, M. R., Rouillard, A. D., Fernandez, N. F., Duan, Q., Wang, Z., Koplev, S., Jenkins, S. L., Jagodnik, K. M., Lachmann, A. et al. (2016) 'Enrichr: a comprehensive gene set enrichment analysis web server 2016 update', *Nucleic Acids Res* 44(W1): W90-7.

Lai, H. C., Seal, R. P. and Johnson, J. E. (2016) 'Making sense out of spinal cord somatosensory development', *Development* 143(19): 3434-3448.

Langlois, S. D., Morin, S., Yam, P. T. and Charron, F. (2010) 'Dissection and culture of commissural neurons from embryonic spinal cord', *J Vis Exp*(39).

Le Dreau, G., Escalona, R., Fueyo, R., Herrera, A., Martinez, J. D., Usieto, S., Menendez, A., Pons, S., Martinez-Balbas, M. A. and Marti, E. (2018) 'E proteins sharpen neurogenesis by modulating proneural bHLH transcription factors' activity in an E-box-dependent manner', *Elife* 7.

Lee, M., Yoon, J., Song, H., Lee, B., Lam, D. T., Baek, K., Clevers, H. and Jeong, Y. (2017) 'Tcf7l2 plays crucial roles in forebrain development through regulation of thalamic and habenular neuron identity and connectivity', *Dev Biol* 424(1): 62-76.

Li, X., Zhao, X., Fang, Y., Jiang, X., Duong, T., Fan, C., Huang, C. C. and Kain, S. R. (1998) 'Generation of destabilized green fluorescent protein as a transcription reporter', *J Biol Chem* 273(52): 34970-5.

Lipiec, M. A., Bem, J., Koziński, K., Chakraborty, C., Urban-Ciećko, J., Zajkowski, T., Dąbrowski, M., Szewczyk Ł, M., Toval, A., Ferran, J. L. et al. (2020) 'TCF7L2 regulates postmitotic differentiation programmes and excitability patterns in the thalamus', *Development* 147(16).

Long, H., Sabatier, C., Ma, L., Plump, A., Yuan, W., Ornitz, D. M., Tamada, A., Murakami, F., Goodman, C. S. and Tessier-Lavigne, M. (2004) 'Conserved roles for Slit and Robo proteins in midline commissural axon guidance', *Neuron* 42(2): 213-23.

Lyuksyutova, A. I., Lu, C. C., Milanesio, N., King, L. A., Guo, N., Wang, Y., Nathans, J., Tessier-Lavigne, M. and Zou, Y. (2003) 'Anterior-posterior guidance of commissural axons by Wnt-frizzled signaling', *Science* 302(5652): 1984-8.

Mambetisaeva, E. T., Andrews, W., Camurri, L., Annan, A. and Sundaresan, V. (2005) 'Robo family of proteins exhibit differential expression in mouse spinal cord and Robo-Slit interaction is required for midline crossing in vertebrate spinal cord', *Dev Dyn* 233(1): 41-51.

Mi, H., Muruganujan, A., Ebert, D., Huang, X. and Thomas, P. D. (2019) 'PANTHER version 14: more genomes, a new PANTHER GO-slim and improvements in enrichment analysis tools', *Nucleic Acids Res* 47(D1): D419-D426.

Morenilla-Palao, C., López-Cascales, M. T., López-Atalaya, J. P., Baeza, D., Calvo-Díaz, L., Barco, A. and Herrera, E. (2020) 'A Zic2-regulated switch in a noncanonical Wnt/βcatenin pathway is essential for the formation of bilateral circuits', *Sci Adv* 6(46).

Moreno-Bravo, J. A., Roig Puiggros, S., Mehlen, P. and Chédotal, A. (2019) 'Synergistic Activity of Floor-Plate- and Ventricular-Zone-Derived Netrin-1 in Spinal Cord Commissural Axon Guidance', *Neuron* 101(4): 625-634.e3.

Morgan-Smith, M., Wu, Y., Zhu, X., Pringle, J. and Snider, W. D. (2014) 'GSK-3 signaling in developing cortical neurons is essential for radial migration and dendritic orientation', *Elife* 3: e02663.

Muroyama, Y., Fujihara, M., Ikeya, M., Kondoh, H. and Takada, S. (2002) 'Wnt signaling plays an essential role in neuronal specification of the dorsal spinal cord', *Genes Dev* 16(5): 548-53.

Myers, J. P. and Gomez, T. M. (2011) 'Focal adhesion kinase promotes integrin adhesion dynamics necessary for chemotropic turning of nerve growth cones', *J Neurosci* 31(38): 13585-95.

Nusse, R. and Clevers, H. (2017) 'Wnt/β-Catenin Signaling, Disease, and Emerging Therapeutic Modalities', *Cell* 169(6): 985-999.

Onishi, K. and Zou, Y. (2017) 'Sonic Hedgehog switches on Wnt/planar cell polarity signaling in commissural axon growth cones by reducing levels of Shisa2', *Elife* 6.

Patthey, C., Tong, Y. G., Tait, C. M. and Wilson, S. I. (2017) 'Evolution of the functionally conserved DCC gene in birds', *Sci Rep* 7: 42029.

Phan, K. D., Croteau, L. P., Kam, J. W., Kania, A., Cloutier, J. F. and Butler, S. J. (2011) 'Neogenin may functionally substitute for Dcc in chicken', *PLoS One* 6(7): e22072.

Reeber, S. L., Sakai, N., Nakada, Y., Dumas, J., Dobrenis, K., Johnson, J. E. and Kaprielian, Z. (2008) 'Manipulating Robo expression in vivo perturbs commissural axon pathfinding in the chick spinal cord', *J Neurosci* 28(35): 8698-708.

Renier, N., Wu, Z., Simon, D. J., Yang, J., Ariel, P. and Tessier-Lavigne, M. (2014) 'iDISCO: a simple, rapid method to immunolabel large tissue samples for volume imaging', *Cell* 159(4): 896-910.

Rhee, J., Buchan, T., Zukerberg, L., Lilien, J. and Balsamo, J. (2007) 'Cables links Robo-bound Abl kinase to N-cadherin-bound beta-catenin to mediate Slit-induced modulation of adhesion and transcription', *Nat Cell Biol* 9(8): 883-92.

Rhee, J., Mahfooz, N. S., Arregui, C., Lilien, J., Balsamo, J. and VanBerkum, M. F. (2002) 'Activation of the repulsive receptor Roundabout inhibits N-cadherin-mediated cell adhesion', *Nat Cell Biol* 4(10): 798-805.

Rousso, D. L., Pearson, C. A., Gaber, Z. B., Miquelajauregui, A., Li, S., Portera-Cailliau, C., Morrisey, E. E. and Novitch, B. G. (2012) 'Foxp-mediated suppression of N-cadherin regulates neuroepithelial character and progenitor maintenance in the CNS', *Neuron* 74(2): 314-30.

Ruiz de Almodovar, C., Fabre, P. J., Knevels, E., Coulon, C., Segura, I., Haddick, P. C., Aerts, L., Delattin, N., Strasser, G., Oh, W. J. et al. (2011) 'VEGF mediates commissural axon chemoattraction through its receptor Flk1', *Neuron* 70(5): 966-78.

Saade, M., Gutierrez-Vallejo, I., Le Dreau, G., Rabadan, M. A., Miguez, D. G., Buceta, J. and Marti, E. (2013) 'Sonic hedgehog signaling switches the mode of division in the developing nervous system', *Cell Rep* 4(3): 492-503.

Sagner, A., Gaber, Z. B., Delile, J., Kong, J. H., Rousso, D. L., Pearson, C. A., Weicksel, S. E., Melchionda, M., Mousavy Gharavy, S. N., Briscoe, J. et al. (2018) 'Olig2 and Hes regulatory dynamics during motor neuron differentiation revealed by single cell transcriptomics', *PLoS Biol* 16(2): e2003127.

Serafini, T., Colamarino, S. A., Leonardo, E. D., Wang, H., Beddington, R., Skarnes, W. C. and Tessier-Lavigne, M. (1996) 'Netrin-1 is required for commissural axon guidance in the developing vertebrate nervous system', *Cell* 87(6): 1001-14.

Ueno, H., Nakajo, N., Watanabe, M., Isoda, M. and Sagata, N. (2008) 'FoxM1-driven cell division is required for neuronal differentiation in early Xenopus embryos', *Development* 135(11): 2023-30.

Wang, H., Lei, Q., Oosterveen, T., Ericson, J. and Matise, M. P. (2011) 'Tcf/Lef repressors differentially regulate Shh-Gli target gene activation thresholds to generate progenitor patterning in the developing CNS', *Development* 138(17): 3711-21.

Wong, G. K., Baudet, M. L., Norden, C., Leung, L. and Harris, W. A. (2012) 'Slit1b-Robo3 signaling and N-cadherin regulate apical process retraction in developing retinal ganglion cells', *J Neurosci* 32(1): 223-8.

Woodhead, G. J., Mutch, C. A., Olson, E. C. and Chenn, A. (2006) 'Cell-autonomous beta-catenin signaling regulates cortical precursor proliferation', *J Neurosci* 26(48): 12620-30.

Wu, Z., Makihara, S., Yam, P. T., Teo, S., Renier, N., Balekoglu, N., Moreno-Bravo, J. A., Olsen, O., Chédotal, A., Charron, F. et al. (2019) 'Long-Range Guidance of Spinal Commissural Axons by Netrin1 and Sonic Hedgehog from Midline Floor Plate Cells', *Neuron* 101(4): 635-647.e4.

Xie, Z., Bailey, A., Kuleshov, M. V., Clarke, D. J. B., Evangelista, J. E., Jenkins, S. L., Lachmann, A., Wojciechowicz, M. L., Kropiwnicki, E., Jagodnik, K. M. et al. (2021) 'Gene Set Knowledge Discovery with Enrichr', *Curr Protoc* 1(3): e90.

Xu, K., Wu, Z., Renier, N., Antipenko, A., Tzvetkova-Robev, D., Xu, Y., Minchenko, M., Nardi-Dei, V., Rajashankar, K. R., Himanen, J. et al. (2014) 'Neural migration. Structures of netrin-1 bound to two receptors provide insight into its axon guidance mechanism', *Science* 344(6189): 1275-9.

Yang, C., Li, X., Wang, C., Fu, S., Li, H., Guo, Z., Zhao, S. and Lin, J. (2016) 'N-cadherin regulates beta-catenin signal and its misexpression perturbs commissural axon projection in the developing chicken spinal cord', *J Mol Histol* 47(6): 541-554.
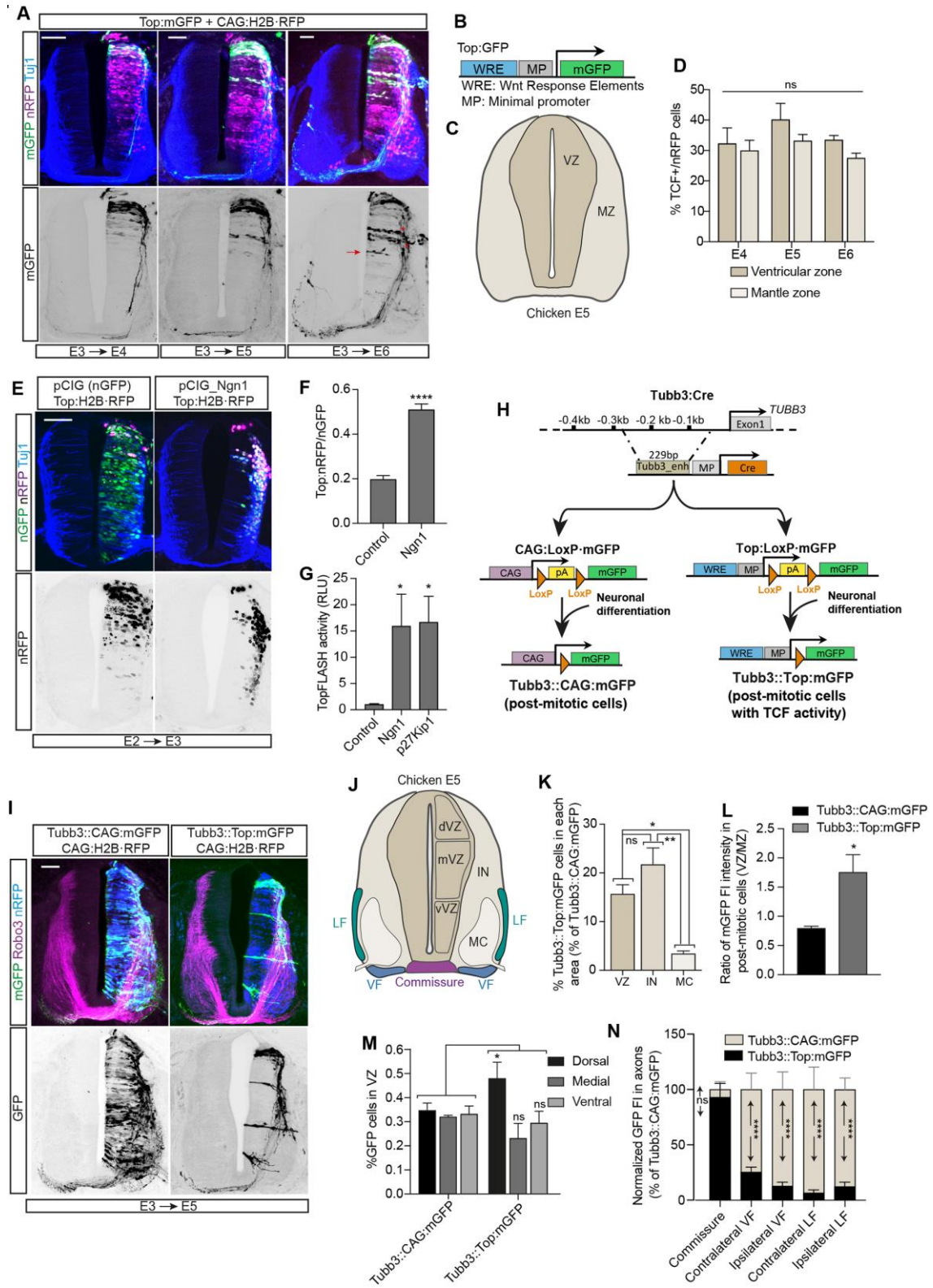
Figures

Fig. 1. Tcf/Lef dependent transcription is activated during commissural differentiation in the chick SC. (A) E3 chick NTs electroporated for 24, 48, or 72 h (E3 + 24 or 48 or 24 h) with Top:mGFP and CAG:H2B·RFP that respectively show Tcf activity (membrane, green) and transfection (nuclear, magenta), transverse slices were stained with Tuj1 antibody (labels neurons, blue). The red arrow points to ventricular Top+ cells out of the Wnt response domain. Asterisks mark dorsal MZ Top+ neurons. Scale bar = 50 μm. (B) Vector used to detect Tcf/Lef activity. (C) Scheme of areas occupied by the mantle zone (MZ) and the ventricular zone (VZ) in an E5 transverse slice of a thoracic chick SC. (D) Bar-graph showing the percentage of Top$^+$ cells among the electroporated ones in MZ and VZ at 24, 48, or 72 hours post electroporation (hpe). Each data point = 6 slices. (E) E2 chick NTs electroporated for 24 h (E2 + 24 h) with Top:H2B·RFP (nuclear, magenta) plus Ngn1 or its control vector pCIG (nuclear, green). E3 slices were stained with Tuj1 antibody (blue). Scale bar = 50 μm. (F) Bar-graph showing the percentage of Top$^+$ cells among the electroporated ones, in control and Ngn1 transfected embryos. Each data point = 5 slices. (G) Bar-graph shows Top-Flash luciferase activity from E2 embryos electroporated for 24 h (E2 + 24 h) with Top-Flash plus control, Ngn1 or p27^{Kip1}. Each data point = 5 slices. (H) Scheme of the CRE/Lox-based vector system created to monitor or manipulate Tcf activity in post-mitotic neurons. The vectors express mGFP cloned in the second slot of a bicistronic arrangement. (I) E3 chick NTs electroporated for 48 h (E3 + 24 h) with Tubb3::CAG:mGFP (shows all transfected neurons, membrane, green) or Tubb3::Top:mGFP (shows Tcf activity in transfected neurons, membrane, green) and CAG:H2B·RFP (shows nucleus, blue). E5 slices were stained with anti Robo3 antibody (stains commissural axons from the cell body to commissure, magenta). Scale bar = 50 μm. (J) Scheme of the ventricular zone (VZ, sub-divided in dorsal, medial, and ventral areas), interneurons (IN), motor column (MC), lateral funiculus (LF), ventral funiculus (VF), and the commissure in E5 chick SC. (K) Bar-graph showing the percentage of Top$^+$ neurons (Tubb3::Top:mGFP) compared to all transfected neurons (Tubb3::CAG:mGFP) in VZ, IN, and MC (E3 + 24 h). Each data point = 3 slices. (L) Bar-graph showing the ratio between the mGFP fluorescence emitted by neurons in the VZ and MZ, either under the Top promoter or under a constitutive promoter (CAG, E3 + 24 h). Each data point = 10 slices for control and 14 for Top. (M) Bar-graph showing the percentage of Top$^+$ neurons (Tubb::Top:mGFP) compared to all transfected neurons (Tubb3::CAG:mGFP) in the dorsal, medial and ventral regions of the ventricular zone

of E3 embryos transfected for 24 h (E3 + 24 h). Each data point = 4 slices for control and 11 for Top. (N) Bar graph showing the relative fluorescence intensity of mGFP measured in the axons of commissure, contralateral VF, ipsilateral VF, contralateral LF, and ipsilateral LF from E3 embryos electroporated for 48 h (E3 + 24 h), comparing Tubb3::Top:mGFP to Tubb::CAG:mGFP. Each data point = 11 slices for control and 14 for Top. The bar-graphs show the mean ± SEM . * = p <0.05, ** = p <0.01, **** = p <0.0001, ns: non-significant.
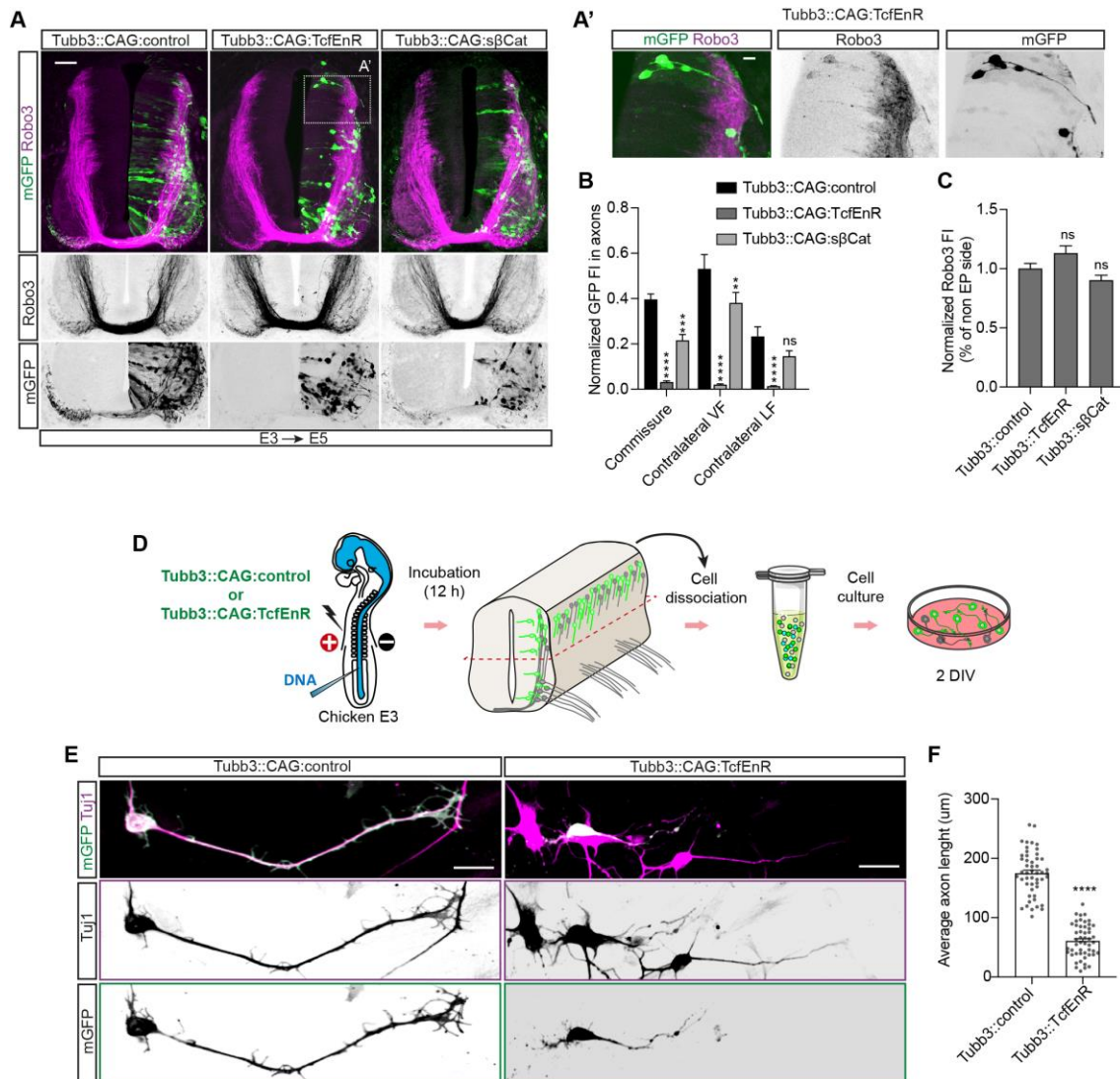
Fig 2. Tcf-Lef-dependent transcription is required for commissural outgrowth and pathfinding in developing SC. (A) E3 chick NTs electroporated for 48 h (E3 + 24 h) with Tubb3::CAG:control, Tubb3::CAG:TcfEnR or Tubb3::CAG:sβ-Cat. mGFP indicates transfected neurons (membrane, green). Transverse sections were stained with an anti-Robo3 antibody (magenta). The area enclosed by the dotted line in A is enlarged in A'. Scale bar =50 μm in A and 10 μm in A'. (B) Bar-graph showing normalized fluorescence intensity of mGFP measured in the axons of commissure, contralateral VF, or contralateral LF from E3 embryos electroporated for 48 h (E3 + 24 h) with Tubb3::CAG:control, Tubb3::CAG:TcfEnR or Tubb3::CAG:sβ-Cat. Each data point = 14 slices for control, 21 for TcfEnR and 20 for sb-Cat (C) Bar-graph showing the ratio between electroporated and non-electroporated sides of normalized Tuj1 fluorescence intensity from E3 embryos transfected for 24 h (E3 + 24 h) with Tubb3::CAG:control, Tubb3::CAG:TcfEnR or Tubb3::CAG:sβ-Cat. Each data point = 3 slices for control, 7

for TcfEnR or 5 for sb-Cat (D) Scheme of the procedure followed to prepare cultures of interneurons transfected with Tubb3::CAG:control or Tubb3::CAG:TcfEnR. (E) Representative images of interneurons transfected with Tubb3::CAG:control or Tubb3::CAG:TcfEnR stained with Tuj1 antibody (magenta), mGFP indicates transfection (membrane, green). Scale bar = 15 μm. (F) Bar-graph showing the average axon length of cultured interneurons transfected with Tubb3::CAG:control or Tubb3::CAG:TcfEnR after 2 days in vitro (DIV). Point = 50 axons from 3 culture wells. The bar-graphs show the mean ± SEM . ** = p <0.01, *** = p <0.001, **** = p <0.0001, ns: non-significant.
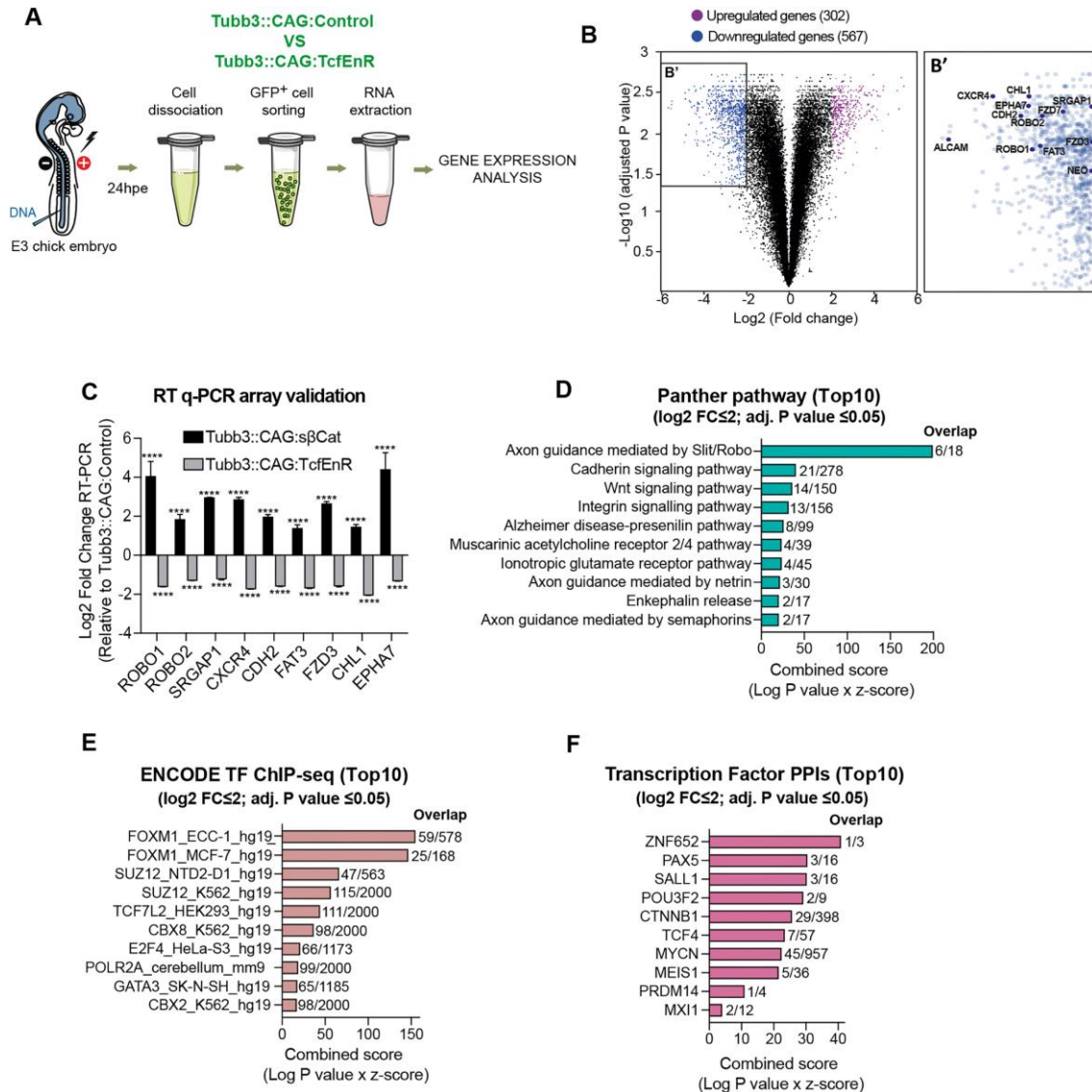
Fig 3. Neural-differentiation-activated Tcf-Lef transcription (DATT) promotes commissural axon elongation and pathfinding through adhesion and axon guidance pathways. (A) Scheme of the procedure followed to study the Tcf/Lef-dependent genes that are active during neural differentiation. (B) Volcano plot showing the corrected gene expression (total abundance and relative variation), comparing embryos transfected with Tubb3::CAG:control to Tubb3::CAG:TcfEnR. Variations superior to four-fold with q values lower than 0.05 were considered significant. Downregulated and upregulated transcripts are highlighted in blue and magenta, respectively [log2 fold change] $\geqq$ 2 with adjusted p value $\leqq$ 0.05. B' shows a magnification of the downregulated genes highlighting a group of 11 manually selected genes involved in diverse aspects of neural differentiation. Each data point = 3 independent PCRs. (C) Validation of the experimental approach by assessing the

expression of a group of very-relevant genes by RT q-PCR, comparing embryos transfected with Tubb::CAG:TcfEnR (Tcf/Lef activity suppressed in neurons), to embryos transfected with Tubb3::CAG:sβ-Cat (Tcf/Lef activity constitutively activated in neurons). (D) Bar-graph showing the combined score of the 10-top Panther pathways that were changed by Tcf/Lef activity suppression in neurons. (E) Bar-graph showing the combined score of the 10-top transcription factors intervening based on ENCODE TF ChiP-seq database. (F) Bar-graph showing the combined score of the 10-top proteins interacting with the implicated transcription factors based on the Transcription Factor PPIs database. The bar-graphs show the mean ± SEM . **** = p <0.0001.
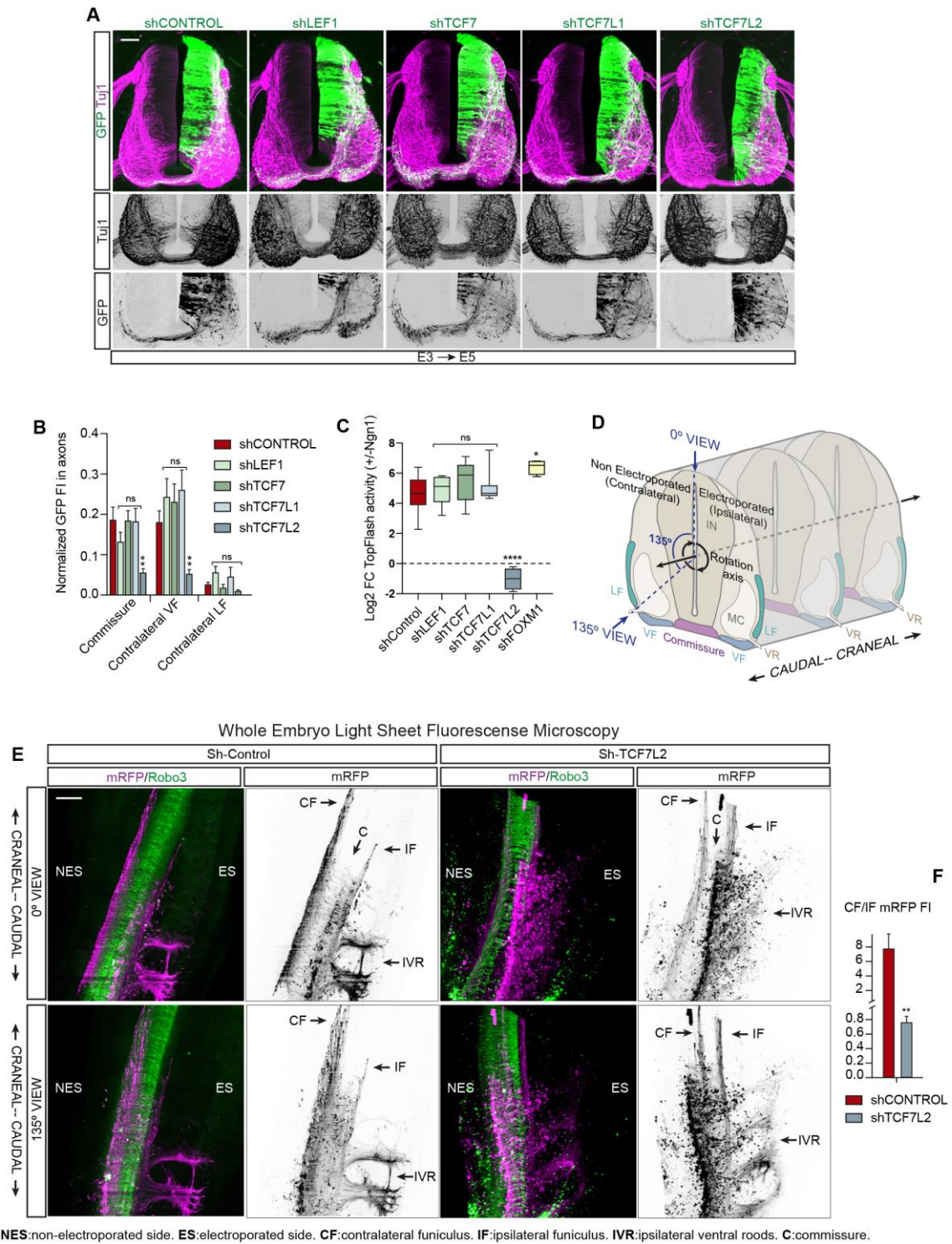
Fig 4. DATT is mediated by TCF7L2 (A) E3 chick NTs electroporated for 48 h (E3 + 24 h) with GFP-expressing pSHIN vectors encoding shRNAs targeting LEF1, TCF7, TCF7L1, or TCF7L2. SC transverse sections were stained with Tuj1 antibody (magenta), and GFP indicates transfection (green). Scale bar = 50 μm. (B) Bar-graph showing normalized fluorescence intensity of mGFP measured in the axons of commissure, contralateral VF, or contralateral LF from E3 chick NTs electroporated for

48 h (E3 + 24 h) with pSHIN vectors encoding shRNAs against LEF1, TCF7, TCF7L1 or TCF7L2. Each data point = 14 slices for control, 11 for LEF1, 13 for TCF7, 9 for TCFL1 and 12 for TCFL2 (C) Bar-graph showing the ratio variation (Log2 FC) of TopFlash activity (luciferase) in embryos transfected or not with Ngn1 and pSHIN vectors encoding shRNAs against LEF1, TCF7, TCF7L1, TCF7L2, or FOXM1. Each data point = 16 embryos for control, 6 for LEF1, 7 for TCF7, 7 for TCFL1, 4 for TCFL2 and 4 for FOXM1. (D) Scheme of an E5 SC to assist with Fig 4E and 3D-images interpretation. IN: interneurons, MC: motor column, LF: lateral funiculus, VF: ventral funiculus, VR: ventral root. (E) Maximum Intensity Projections using 0º and 135º perspectives of 360º images generated from cleared E3 chick embryos electroporated for 24 h (E3 + 24 hpe) with pCS2-mRFP plus pSHIN-ShTCF7L2 or pSHIN-ShControl that were whole-mount immuno labeled with anti RFP (magenta) and anti Robo3 (green) antibodies. Volume imaging was performed through light sheet fluorescence microscopy at 9.6x. Scale bar = 250 μm. (F) Bar-graph showing the ratio of fluorescence intensity of mRFP measured in the axons of ipsilateral and contralateral ventral funiculus measured in two embryos for each condition. The bar-graphs show the mean ± SEM . * = $p < 0.05$, ** = $p < 0.01$, **** = $p < 0.0001$, ns: non-significant.
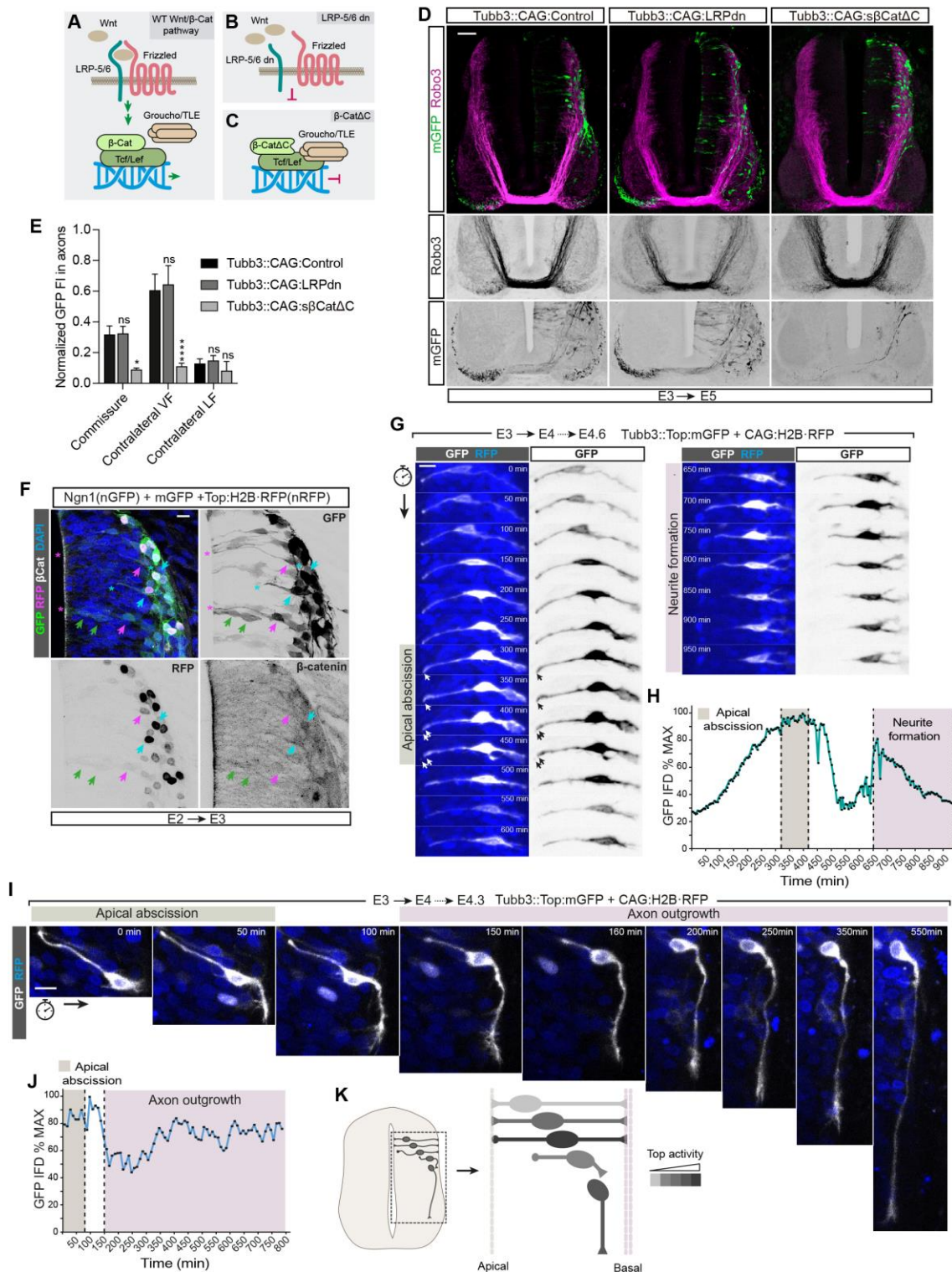
Fig 5. DATT is Frizzled independent and begins before apical abscission. (A-C)
Schemes of wild-type canonical Wnt pathway, dominant negative LRP 5/6 with a C-
terminal deletion and β-catenin with a C-terminal deletion. (D) E3 chick NTs
electroporated for 48 h (E3 + 24 h) with Tubb3::CAG:control, Tubb3::CAG:LRPdn or
Tubb3::CAG:sβ-CatΔC. Transverse sections were stained with anti Robo3 antibody

(magenta), mGFP is expressed by transfected neurons (membrane, green). Scale bar = 50 μm. (E) Bar-graph showing normalized mGFP fluorescence intensity measured in the axons of the commissure, contralateral VF, and contralateral LF from E3 chick NTs electroporated for 48 h (E3 + 24 h) with Tubb3::CAG:control, Tubb3::CAG:LRPdn or Tubb3::CAG:sβ-CatΔC. Each data point = 6 slices for control, 9 for LRPdn or 8 for sb-CatΔC. (F) Transverse sections of E2 chick NTs electroporated for 24 h (E2 + 24 h) with Ngn1 (nuclear GFP, green), membrane GFP (green) and Top::H2B·RFP (nuclear RFP, magenta). Nuclei are indicated by arrows and the apical processes by stars. Green arrows/stars show cells whose nucleus is close to the apical border and have NSC morphology, purple arrows/stars indicate cells with the nucleus occupying basal positions but with the apical process still attached to the apical border, and blue arrows/stars indicate cells in which the apical abscission has already occurred. Scale bar = 10 μm. (G) Representative images of E3 chick NTs transfected for 24 h with Tubb3::Top:mGFP and cultured ex vivo for 950 min (E3 + 24 h + 950 min). mGFP levels reflect Top activity in neurons. Scale bar = 10 μm. (H) The plot shows the integrated GFP fluorescence density (IFD) of the cell shown in G calculated from flattened images of the Z-planes containing the entire cell at each time point. Images were taken every 5 min. The shaded areas indicate the periods in which the apical abscission and neurite formation took place. (I) A similar experiment as in H, but following a cell in which the apical abscission had already started when the time laps were initiated. Images were taken every 10 min. Scale bar = 10 μm. (J) Plot showing the GFP fluorescence intensity of the cell shown in I. (K) Schematic representation in grey-scale code of Top activity along neuron differentiation. The bar-graphs show the mean ± SEM . * = p <0.05, **** = p <0.0001, ns: non-significant.
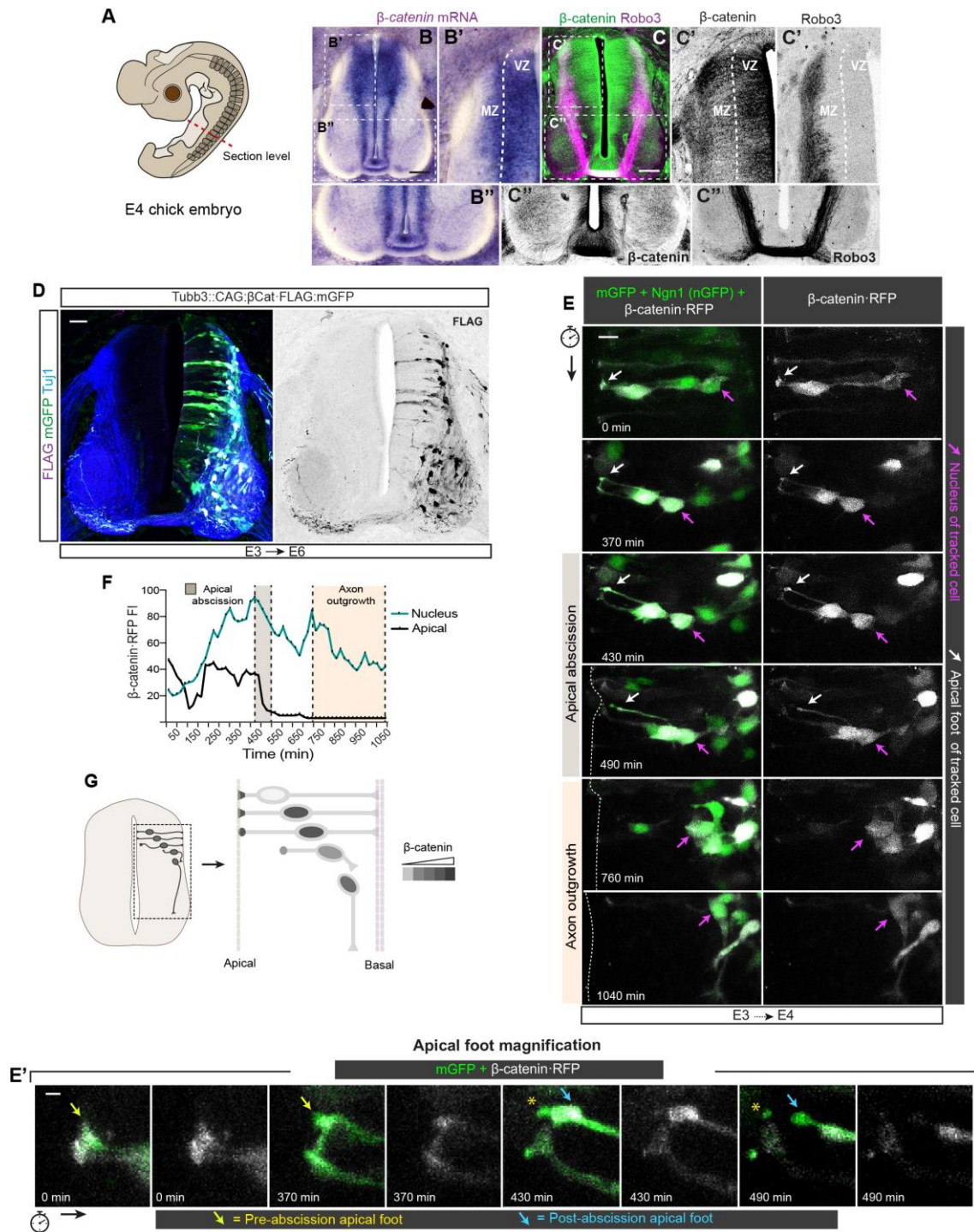
Fig 6. β-catenin is readdressed to the nucleus before apical foot abscission during neural differentiation. (A) Drawing of an E4 chick embryo indicating the approximate thoracic level used to generate the transverse sections used in this work. (B) In situ hybridization showing CTNNB1 mRNA distribution in transverse sections of E4 chick SC. The areas labeled as B' and B'' are enlarged in the right-handed and bottom panels, respectively. Scale bar = 50 μm. (C) E4 SC sections stained with anti-β-catenin (green)

and anti Robo3 (magenta). The areas labeled as C' and C'' are enlarged in the right-handed and bottom panels, respectively, in this case β-catenin and Robo3 stainings are shown separately in a grey scale. Scale bar = 50 μm. (D) E3 embryos electroporated for 72 h (E3 + 24 h) with Tubb3::CAG:βCat·FLAG:mGFP (express β-catenin·FLAG in neurons) stained with anti FLAG antibodies (magenta) and Tuj1 (blue). FLAG staining is shown alone in greyscale at the right-handed panel. Scale bar = 50 μm. (E) Representative images of E2 chick NTs transfected for 24 h with mGFP (membrane, green), Ngn1 (nuclear GFP, green), and β-catenin·RFP (greyscale) and cultured ex vivo for 1040 min (E2 + 24 h + 1040 min). RFP signal is shown alone in greyscale in the right-handed panels. In each time-lapse, the position of the apical process and the nucleus of the tracked cell are indicated by white and magenta arrows, respectively. Scale bar = 10 μm. E' panel (at the bottom) presents magnified images of mGFP (green) and β-catenin·RFP (greyscale) distribution in the apical foot during apical abscission. Pre and post-abscission apical feet are respectively indicated by yellow and blue arrows. The membrane stump left behind after abscission is indicated by yellow stars. Scale bar = 2 μm. (F) The plot shows the RFP fluorescence intensity measured in the apical foot (black line) and the nucleus (green line) at each time point. Images were taken every 10 min. The shaded areas indicate the periods in which the apical abscission and axon outgrowth took place. (G) The drawing shows a schematic representation of β-catenin·RFP distribution (in grey-scale code) along neuron differentiation.
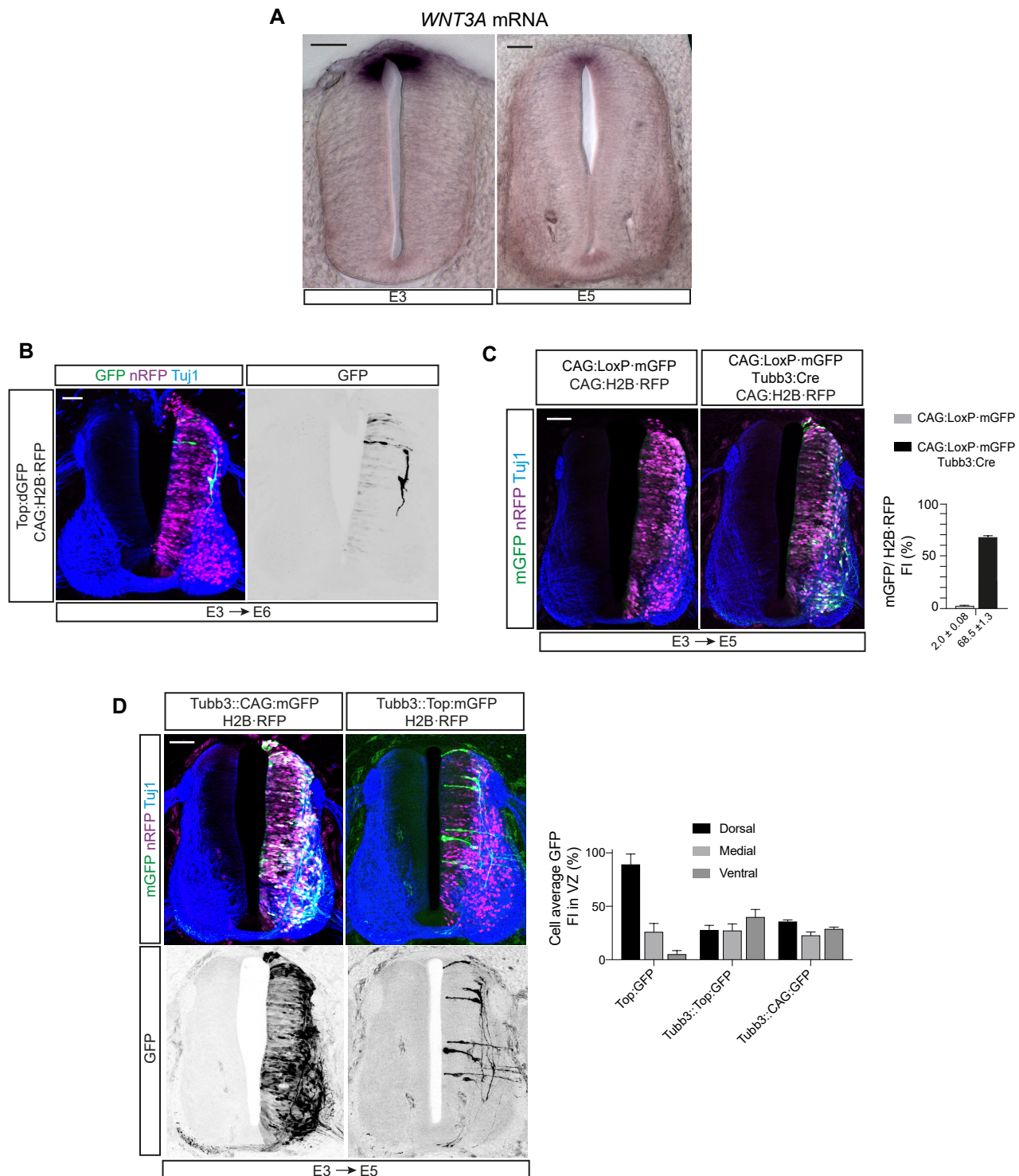
Fig. S1. (A) In situ hybridization showing *WNT3A* mRNA distribution in transverse sections of E3 and E5 chick SC. Scale bar = 50 μm. (B) E3 chick NTs electroporated for 72 h (E3 + 24 h) with Top:dGFP (destabilized GFP, green) and CAG:H2B·RFP (nuclear RFP, magenta). Transverse SC slices were stained with Tuj1 antibody (blue). dGFP is shown alone in greyscale at the right-handed panel. (C) E3 chick NTs electroporated for 48 h (E3 + 24 h) with CAG:LoxP·GFP plus CAG:H2B·RFP without (left panel) or with (right panel) Tubb3:Cre. The bar-graph shows the ratio of fluorescence intensity between mGFP and H2BRFP in ventricular zone (D) E3 chick NTs electroporated for 48 h (E3 + 24 h) with Tubb3::CAG:mGFP (shows all transfected neurons, membrane, green) or Tubb3::Top:mGFP (shows the Tcf/Lef activity in transfected neurons, membrane, green) and CAG:H2B·RFP (shows nucleus, magenta). E5 transverse SC slices were stained with anti Tuj1 antibody (stains all neurons, blue). The bar-graph shows the mean GFP fluorescence intensity in the dorsal, medial and ventral ventricular zone in neural tubes with the indicated transfections.
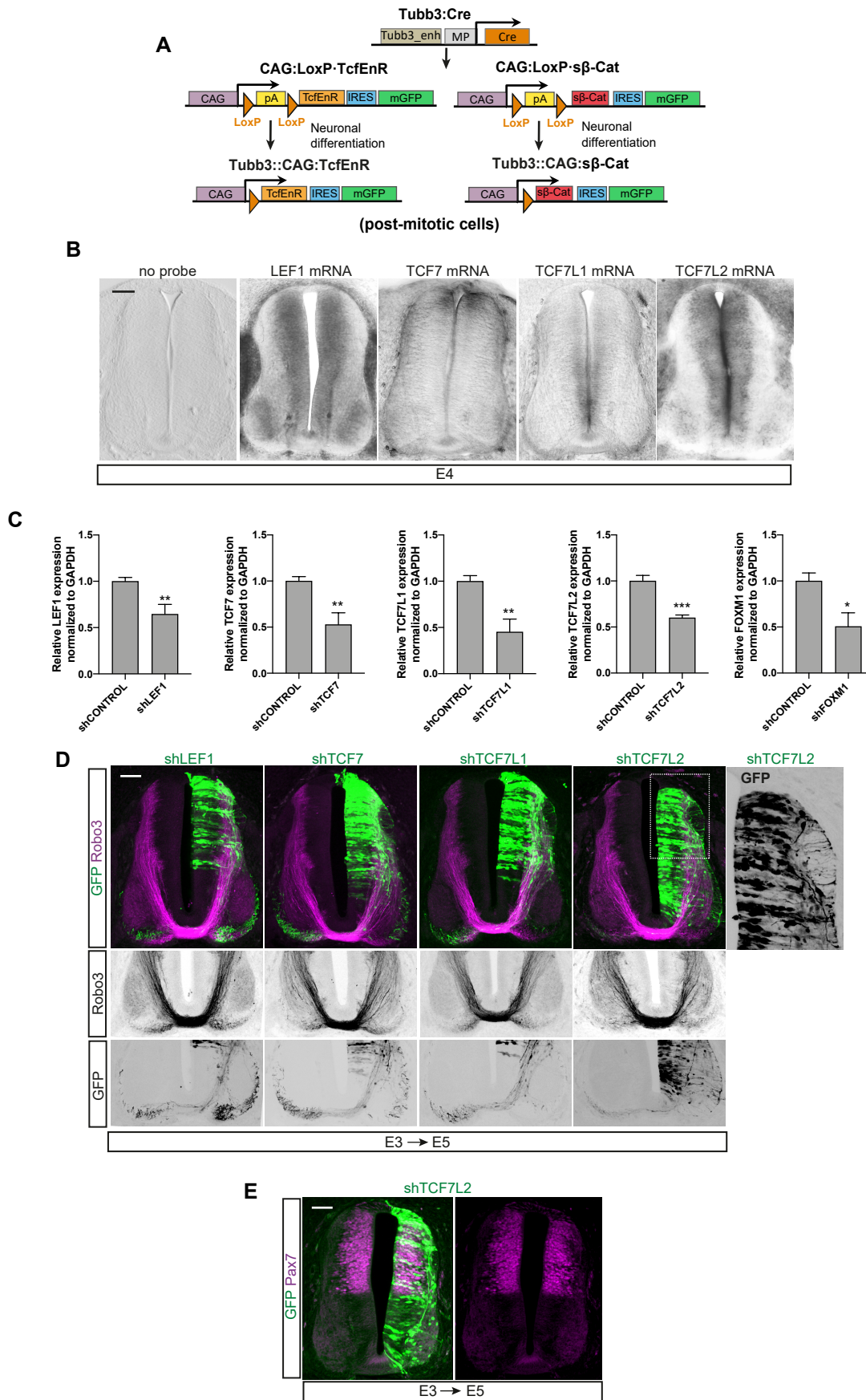
Fig. S2. (A) Scheme of vectors used to generate Tubb3::CAG:TcfEnR and Tubb3::CAG:sβ-Cat embryos. (B) In situ hybridization showing in grey scale LEF1, TCF7, TCF7L1 or TCF7L2 mRNA distribution in transverse sections of E4 chick SC. (C) Bar-graph showing the efficiency of the different short-hairpin inhibitory RNAs (shRNAs) designed against the different Tcf/Lef transcription factors expressed in chick NTs and FOXM1. The shRNAs were cloned in the GFP expressing vector pSHIN and tested in chick embryonic fibroblast cultures by RT qPCR. (D) E3 chick NTs electroporated for 48 h (E3 + 24 h) with GFP-expressing pSHIN vectors encoding shRNAs against LEF1, TCF7, TCF7L1, or TCF7L2. SC transverse sections were stained with anti-Robo 3 antibody (magenta), and GFP (green) indicates transfection. The content of the area delimited by a dotted line in the shTCFL2 panel is magnified at the right-handed panel showing in greyscale the GFP channel. (E) E3 chick NTs electroporated for 48 h (E3 + 24 h) with an shRNA targeting TCF7L2 (cloned in pSHIN vector), SC transverse sections were stained with anti Pax7 antibody (an interneuron marker, magenta), GFP (green) indicates transfection.
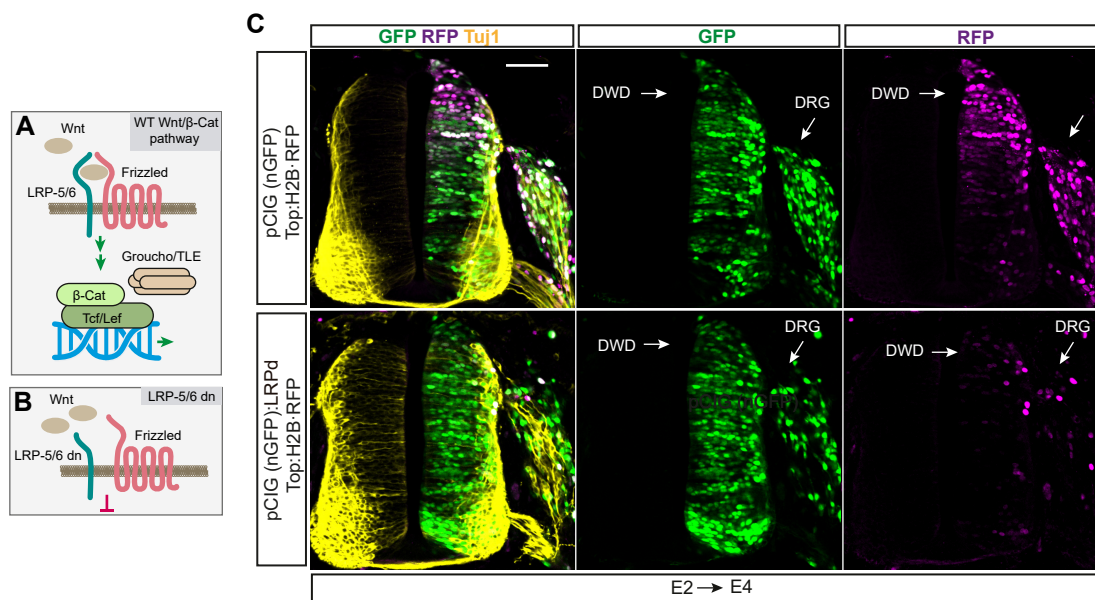
Fig. S3. (A) Simplified scheme illustrating wild-type canonical Wnt pathway where binding of Wnt proteins to Frizzled receptor and its co-receptor LRP 5/6 activates Tcf dependent transcription. (B) The pathway cannot be initiated at receptor level in the presence of a dominant negative form of LRP 5/6 with a C-terminal deletion. (C) E2 chick NTs electroporated for 40 h (E2 + 40 h) with TOP-H2B·RFP (expresses nuclear RFP under a Wnt response element, magenta) plus pCIG-LRPdn (expresses the dominant negative form of LRP5-6 and nuclear GFP as a bicistronic element) or pCIG (green). SC transverse sections were stained with Tuj1 antibody (yellow). In this case we observed that pCIG-LRPdn expression clearly inhibited the expression of TOP-H2B·RFP in the dorsal Wnt response domain and the dorsal root ganglia (DRG), two regions in which endogenous Wnt factors activate Wnt signalling in E2-E4 chick neural tubes.
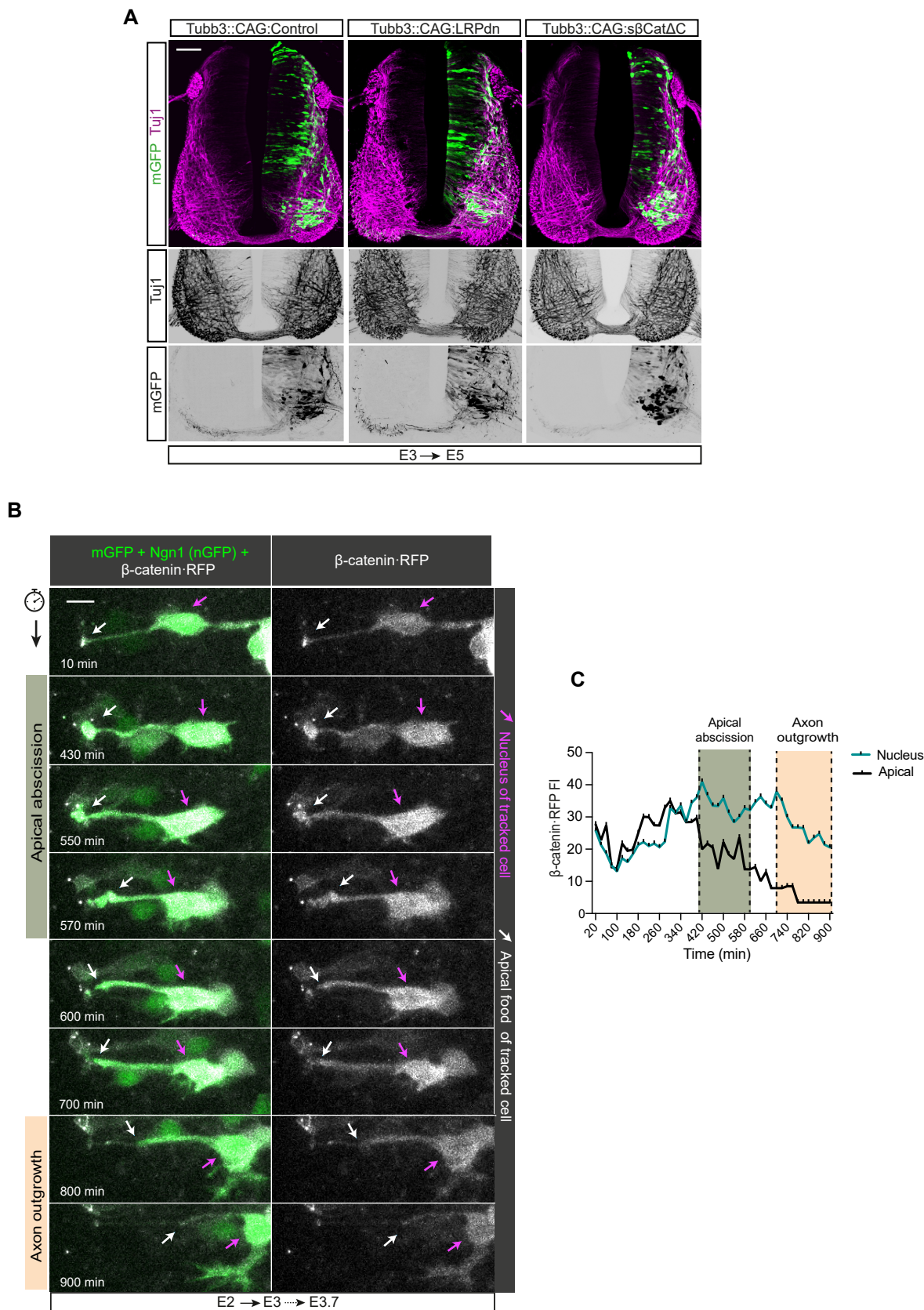
Fig. S4. (A) E3 chick NTs electroporated for 48 h (E3 + 24 h) with Tubb3::CAG:control, Tubb3::CAG:LRPdn or Tubb3::CAG:sβ-CatΔC. Transverse SC slices were stained with Tuj1 antibody (magenta). (B) Representative images of E2 chick NTs transfected for 24 h with mGFP (green, membrane), Ngn1 (green, nuclear GFP indicates transfection), and β-catenin·RFP (greyscale) and cultured ex vivo for 900 min (E2 + 24 h + 900 min). RFP signal is shown alone in greyscale in the right-handed panels. In each time-lapse, the position of the apical process and the nucleus of the tracked cell are indicated by white and magenta arrows, respectively. (C) The plot shows the RFP fluorescence intensity measured in the apical foot (black line) and the nucleus (green line) over time. Images were taken every 10 min. The shaded areas indicate the periods in which the apical abscission and axon outgrowth took place.

Table S1. Tubb3 dependent gene expression. The table contains three separated columns enumerating all the genes processed in the array, the genes that are upregulated and the genes that are downregulated.

Click here to download Table S1

Table S2. Tubb3 dependent gene expression meta data. The table contains the metadata of the Afimetrix gene expression study.

Click here to download Table S2
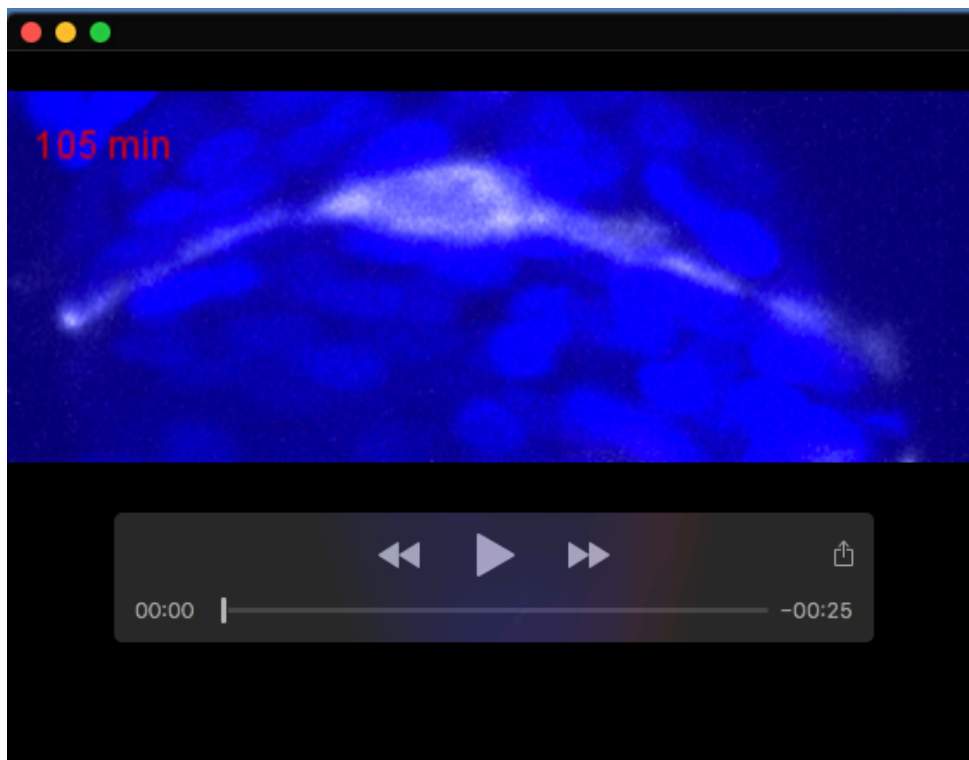
Movie 1. E3 chick NTs transfected for 24 h with Tubb3::Top:mGFP plus CAG:H2b·RFP and cultured ex vivo for 950 min (E3 + 24 h + 950 min). Images were taken every 5 min. mGFP (grey scale) levels reflects Top activity in neurons, nuclear RFP (blue) indicates transfection.
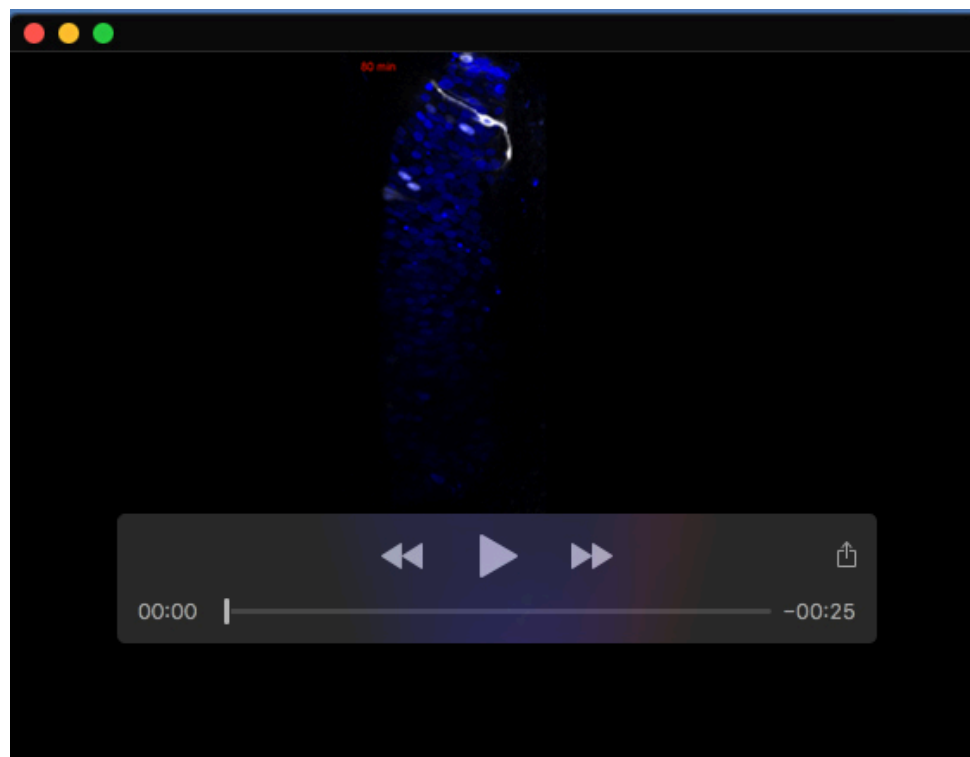

Movie 2. E3 chick NTs transfected for 24 h with Tubb3::Top:mGFP plus CAG:H2b·RFP and cultured ex vivo for 800 min (E3 + 24 h + 800 min). Images were taken every 10 min. mGFP levels reflect Top activity in neurons, nuclear RFP (blue) indicates transfection.
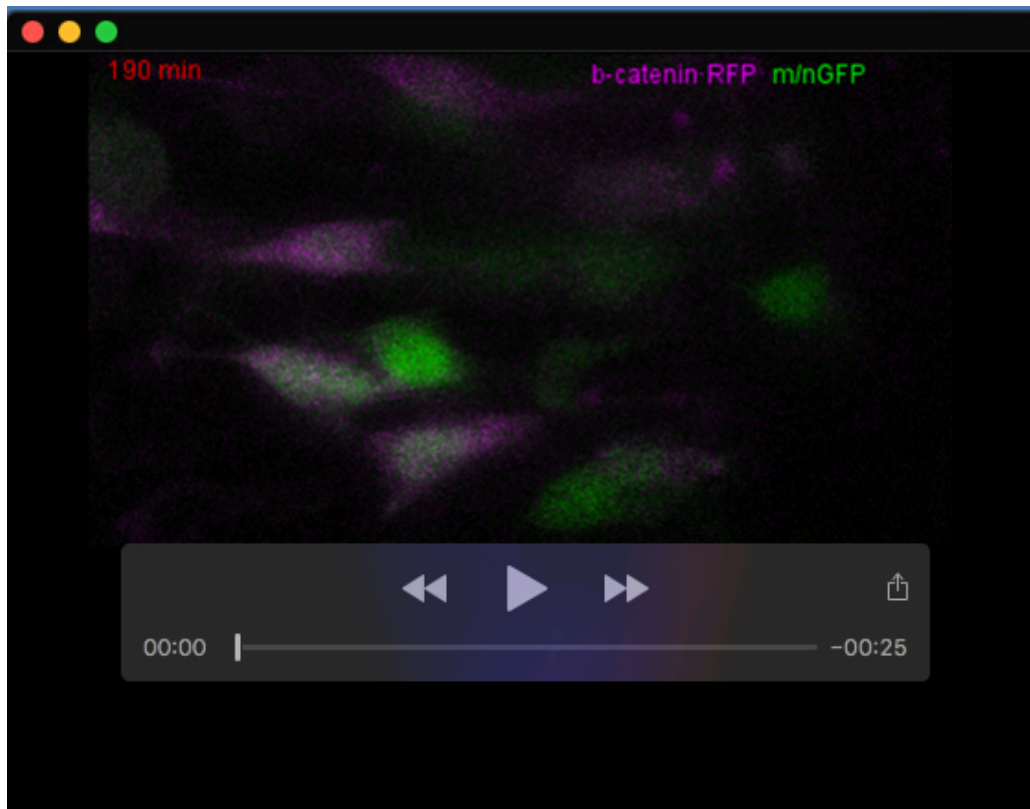
Movie 3. E2 chick NTs transfected for 24 h with mGFP (membrane GFP, green), Ngn1 (nuclear GFP, green) and β-catenin·RFP (magenta) and cultured ex vivo for 1040 min (E2 + 24 h + 1040 min). Following two channel images, β-catenin·RFP channel is shown separately in greyscale. Images were taken every 10 min.
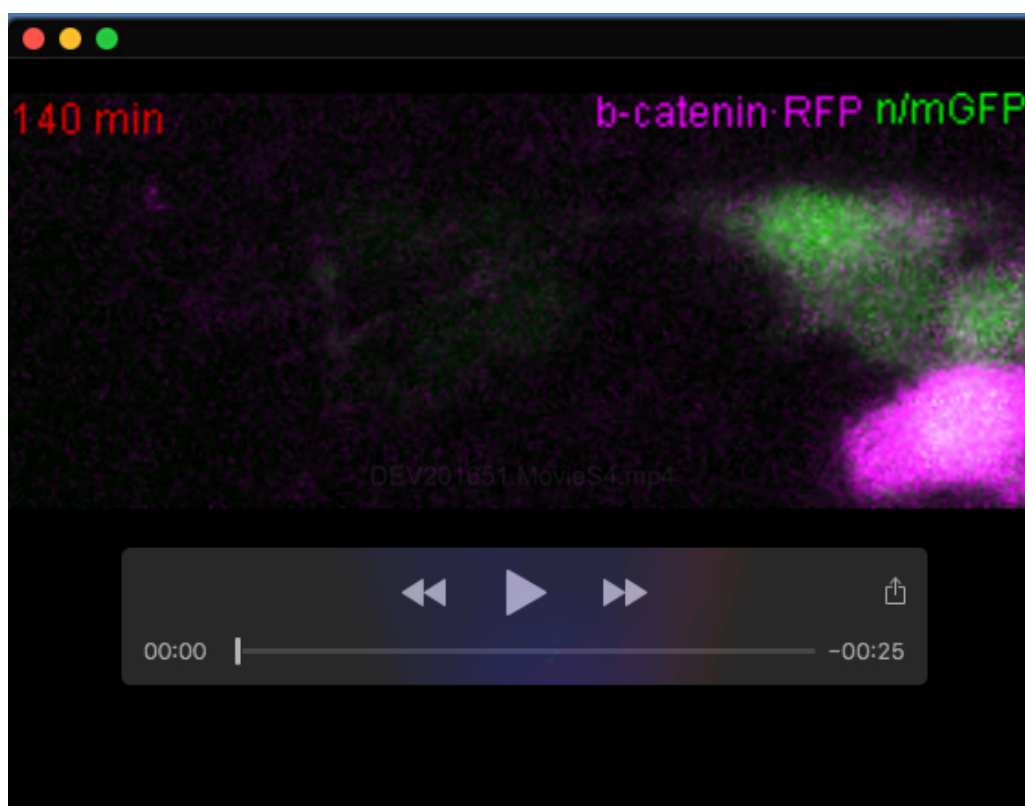
Movie 4. E2 chick NTs transfected for 24 h with mGFP (membrane GFP, green), Ngn1 (nuclear GFP, green), and β-catenin·RFP (magenta) and cultured ex vivo for 900 min (E2 + 24 h + 900 min). Following two channel images, β-catenin·RFP channel is shown separately in greyscale. Images were taken every 10 min.
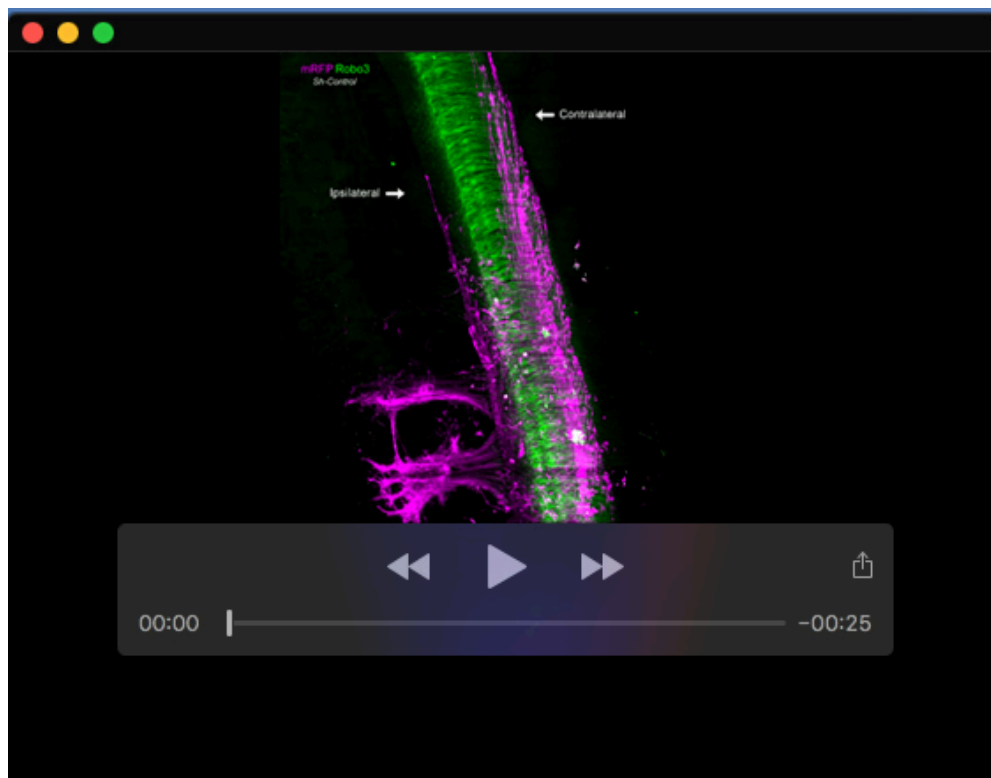
Movie 5. 360º view of 3D reconstruction of volume imaging performed through light sheet fluorescence microscopy at 9.6x of cleared E3 chick embryos electroporated for 24 h (E3 + 24 hpe) with pCS2-mRFP plus pSHIN-ShControl that were whole-mount immuno labeled with anti RFP (magenta) and anti Robo3 (green) antibodies. The RFP channel is shown alone in grey scale after the magenta/green sequence. The image shows 1º steps of a 360º rotation with the axis placed in the cranial-caudal direction. 3D reconstruction was generated with ImageJ/Fiji.
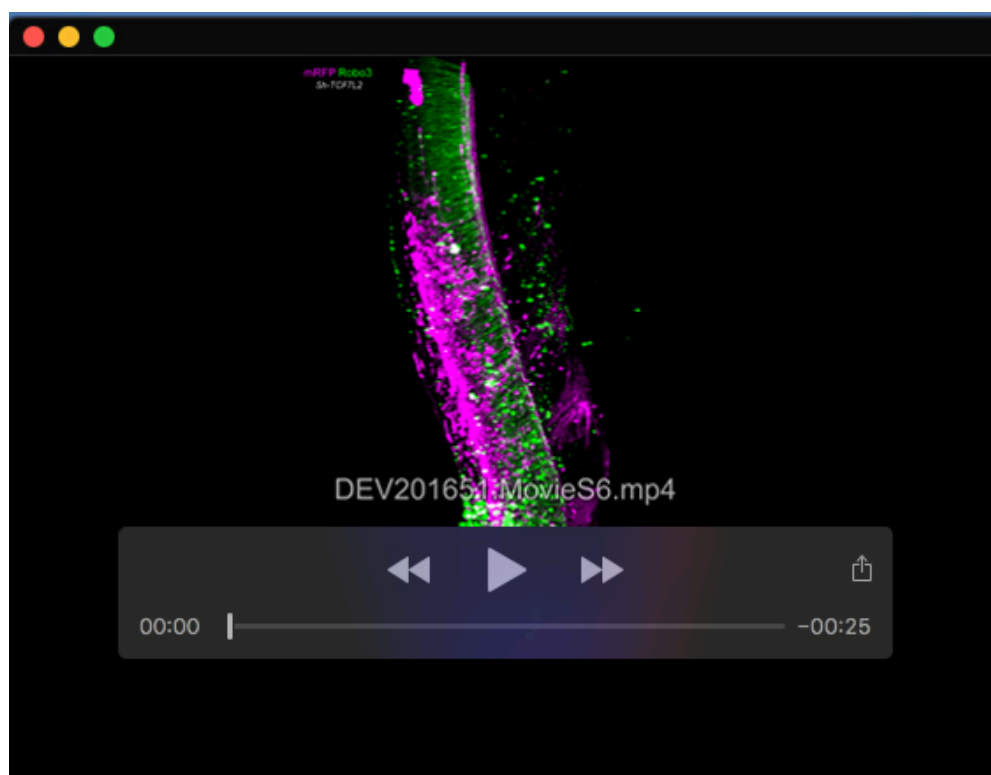
Movie 6. 360º view of 3D reconstruction of volume imaging performed through light sheet fluorescence microscopy at 9.6x of cleared E3 chick embryos electroporated for 24 h (E3 + 24 hpe) with pCS2-mRFP plus pSHIN-ShTCF7L2 that were whole-mount immuno labeled with anti RFP (magenta) and anti Robo3 (green) antibodies. The RFP channel is shown alone in grey scale after the magenta/green sequence. The image shows 1º steps of a 360º rotation with the axis placed in the cranial-caudal direction. 3D reconstruction was generated with ImageJ/Fiji.